Development and growth of the pectoral girdle and fin skeleton in the extant coelacanth Latimeria chalumnae

Rohan Mansuit, Gaël Clément, Anthony Herrel, Marc Herbin, Hugo Dutel, Paul Tafforeau, Mathieu D. Santin

1 **Development and growth of the pectoral girdle and fin skeleton in the extant coelacanth** *Latimeria*

2 *chalumnae*

3 Mansuit Rohan[1, 2], Clément Gaël[1], Herrel Anthony[2], Hugo Dutel[3], Paul Tafforeau[4], Mathieu D. Santin[5]

4 and Herbin Marc[2]

5 [1] UMR 7207 Centre de Recherche en Paléontologie, Paris, MNHN – Sorbonne Université – CNRS,

6 Département Origines & Evolution, Muséum national d'Histoire naturelle, 57 rue Cuvier, 75005 Paris,

7 France

8 [2] UMR 7179 MECADEV, MNHN – CNRS, Département Adaptations du Vivant, Muséum national

9 d'Histoire naturelle, 57 rue Cuvier, 75005 Paris, France

10 [3] School of Earth Sciences, University of Bristol, 24 Tyndall avenue, BS8 1TQ, United-Kingdom.

11 [4] European Synchrotron Radiation Facility, BP 220, 6 Rue Jules Horowitz, 38043 Grenoble Cedex,

12 France.

13 [5] Inserm U 1127, CNRS UMR 7225, Centre for NeuroImaging Research, ICM (Brain & Spine Institute),

14 Sorbonne University, Paris, France

15

16 **Address for correspondence:**

17 Rohan Mansuit

18 UMR 7179 MECADEV, MNHN – CNRS,

19 Département Adaptations du Vivant

20 55 rue Buffon

21 75005 Paris, France   e-mail : rohan.mansuit@mnhn.fr

22   **Abstract**

23   The monobasal pectoral fins of living coelacanths and lungfishes are homologous to the forelimbs of

24   tetrapods and are thus critical to investigate the origin thereof. However, it remains unclear whether

25   the similarity in the asymmetrical endoskeletal arrangement the pectoral fins of coelacanths reflects

26   the evolution of the pectoral appendages in sarcopterygians. Here, we describe for the first time the

27   development of the pectoral fin and shoulder girdle in the extant coelacanth *Latimeria chalumnae*,

28   based on the tomographic acquisition of a growth series. The pectoral girdle and pectoral fin

29   endoskeleton are formed early in the development with a radially outward growth of the endoskeletal

30   elements. The visualization of the pectoral girdle during development shows a reorientation of the

31   girdle between the fetus and pup 1 stages, creating a contact between the scapulocoracoids and the

32   clavicles in the ventro-medial region. Moreover, we observed a splitting of the pre- and post-axial

33   cartilaginous plates in respectively pre-axial radials and accessory elements on one hand, and in post-

34   axial accessory elements on the other hand. The mechanisms involved in the splitting of the

35   cartilaginous plates appear, however, different from those involved in the formation of radials in

36   actinopterygians. Our results show a proportional reduction of the proximal pre-axial radial of the fin

37   rendering the external morphology of the fin more lobe-shaped and a spatial reorganization of

38   elements resulting from the fragmentation of the two cartilaginous plates. *Latimeria* development

39   hence supports previous interpretations of the asymmetrical pectoral fin skeleton as being

40   plesiomorphic for coelacanths and sarcopterygians.

41   **Keywords**

2

Introduction :

Among the sarcopterygians, the clade Actinistia is today only represented by the coelacanth genus *Latimeria*, and is considered as the sister group to the Rhipidistia, represented by living lungfishes and tetrapods (Ahlberg, 1991; Forey, 1998; Friedman *et al.*, 2007; Clack, 2012; Amemiya *et al.*, 2013). This clade presents a long evolutionary history with its origin dating back to the Early Devonian (Johanson *et al.*, 2006; Friedman, 2007; Zhu *et al.*, 2012b). Coelacanths are well represented in the fossil record, with about 40 described genera and more than 130 species (Forey, 1998). The clade also presents an important diversity of form, size and ecology (Forey, 1998; Friedman & Coates, 2006; Casane & Laurenti, 2013; Cavin & Guinot, 2014; Cavin *et al.*, 2017), and was considered to have gone extinct at the end of the Mesozoic Era (Smith, 1939). Today, there are two known species: *Latimeria chalumnae* (Smith, 1939) in Western Indian Ocean and *L. menadoensis* (Erdmann *et al.*, 1998; Pouyaud *et al.*, 1999) discovered offshore of Sulawesi, Indonesia.

Because of their close relationships with tetrapods, many aspects of the biology and development of the coelacanths are of interest to better understand the origin, the anatomical characteristics and the evolution of osteichthyans (Dutel *et al.*, 2019) and early land vertebrates (Fricke & Hissmann, 1992). Pectoral fins of coelacanths are moreover of particular interest, partly due to the fact that the paired fin skeleton of the coelacanth is organized along a metapterygial axis (Millot & Anthony, 1958). This organisation is similar to that of the endochondral skeletal elements of lungfishes, and tetrapod limbs (Shubin & Alberch, 1986; Mabee, 2000). Consequently, the paired lobed-fin of sarcopterygian fishes is considered homologous to the tetrapod limb (i.e. Gregory and Raven, 1941; Westoll, 1943; Fricke and Hissmann, 1992; Clack, 2009). Moreover, the first elements of the pectoral fin of the coelacanth (the first mesomere, the first pre-axial radial, and the second mesomere) are considered to be homologous to the stylopodal and zeugopodal elements of the tetrapod limb (Fricke & Hissmann, 1992; Johanson *et al.*, 2007; Miyake *et al.*, 2016). The majority of studies concerning the water-to-land transition of vertebrates have focused on the pectoral appendages given their importance during locomotion in transitional and early terrestrial vertebrates (Shubin *et al.*, 2006; Pierce *et al.*, 2012; Standen *et al.*, 2014). Coelacanths have also been considered as being relevant in the context of terrestrialization because they move their fins in an alternating manner, reminiscent of the movements of tetrapod limbs (Fricke *et al.*, 1987; Forey, 1998; Clack, 2012). However, the fins of the extant coelacanth clearly do not have a function of "legs", i.e. crawling on sea bottom, as had been supposed by Smith (1956). Whereas lungfishes are more closely related to tetrapods than coelacanths, as early as the beginning of their evolutionary history, they present modified paired fins with a high degree of symmetry that do not reflect the pectoral fin of early sarcopterygians (Ahlberg, 1989; Coates *et al.*, 2002; Coates, 2003; Friedman *et al.*, 2007). One the other hand, early tetrapodomorphs and coelacanths show

77   asymetrical fins (Ahlberg, 1989; Friedman et al., 2007), where the pre-axial and post-axial side of the

78   fin do not have the same arrangement around the metapterygial axis. It remains unknown, however,

79   whether the evolution of the pectoral fin of coelacanths is informative about the evolution of the

80   pectoral appendages in sarcopterygians more generally.

81   The pectoral fin and girdle development of the living coelacanth remains unknown. Consequently, a

82   detailed anatomical description of the morphology and anatomy of the pectoral fin and girdle at

83   different ontogenetic stages of the extant coelacanth is crucial for an understanding of the

84   development of the pectoral fin of *Latimeria* in comparison to fossil coelacanths and tetrapodomorphs.

85   The development of the endoskeleton of the pectoral fin and girdle in *Latimeria* is likely to be

86   informative for reconstructing the plesiomorphic configuration of the pectoral appendages in

87   sarcopterygians (Coates *et al.*, 2002; Amaral & Schneider, 2017). Here, we study the development of

88   the pectoral fin and girdle in the extant coelacanth by describing this anatomical complex in a unique

89   ontogenetic series of five stages constitued of three prenatal stages and two post-natal stages (Dutel

90   *et al.*, 2019).

91   **Materials and methods** :

92   *Specimens*

93   The developmental series includes five stages from several museum collections (Fig. 1). The first stage

94   is a fetus of 5 cm total length (TL) (CCC 202.1) (Nulens *et al.*, 2011) found inside the female specimen

95   CCC 202 captured off the Tanzanian coast in 2005 and conserved in the collection of the South African

96   Institute for Aquatic Biodiversity, Grahamstown, South Africa (SAIAB 76199). Stage 2 is a pup of 32.3

97   cm TL with a yolk sac (CCC 29.5), found inside the female specimen CCC 29 captured off the Comores

98   Island in 1969 and conserved in the collection of the MNHN, Paris, France (MNHN AC 2012-22). Stage

99   3 is a late pup which yolk sac is resorbed of 34.8 cm TL (CCC 162.21) found inside the female CCC 162

100   captured off the coast of Mozambique in 1991, and conserved in the collection of the Zoologische

101   Staatssammlung, Munich, Germany (ZSM 28409). Stage 4 is a juvenile of 42.5 cm TL (CCC 94) captured

102   off Grande Comore in 1974 and conserved in the collection of the MNHN, Paris, France (MNHN AC

103   2012-27). The adult specimen (stage 5) principally used in this study is a male of 130 cm TL (CCC 22)

104   captured in Grande Comore in 1960 and conserved in the collection of the MNHN, Paris, France (MNHN

105   AC 2012-18). Direct anatomical observations were also made on isolated pectoral fin skeleton of

106   several adult specimens: CCC 6 (MNHN AC 2012-4), CCC 7 (MNHN AC 2012-5), CCC 14 (MNHN AC 2012-

107   11) and CCC 19 (MNHN AC 2012-15). Specimens from the MNHN, Paris are preserved in a 6-7%

108   formaldehyde solution, while the others are preserved in a 70 % aquaeous ethanol solution.

109   *Imaging*

110   Stage 1 – Fetus (CCC 202.1)

111 The specimen was scanned using long propagation phase-contrast synchrotron X-ray
112 microtomography at the ID19 beamline of the European Synchrotron Radiation Facility (ESRF),
113 Grenoble (France). It was imaged at a voxel size 6.5 µm using a pink beam achieved with a W150
114 wiggler at a gap of 50 mm and filtered with 2 mm of aluminium, 0.25 mm of copper and 0.2 mm of
115 gold. The scintillator was a 250-µm-thick LuAG:Ce (lutetium–aluminium–garnet) crystal. The resulting
116 detected spectrum was centred on 73 keV with a bandwidth of 17 keV FWHM (full width at half
117 maximum). The detector was a FreLoN 2K14 charge coupled device (CCD) camera mounted on a lens
118 system. To obtain a sufficient propagation phase-contrast effect, a distance of 3m between the sample
119 and the detector was used. The final reconstruction (13µm) was obtained after binning with the
120 software ImageJ.

121   Stage 2 – Pup 1 (with yolk sac) (CCC 29.5)

122 The specimen was scanned using long propagation phase-contrast synchrotron X-ray
123 microtomography at the ID19 beamline of the European Synchrotron Radiation Facility (ESRF),
124 Grenoble (France). It was scanned at a voxel size of 23.34 µm and using a propagation distance of 13m
125 to maximize the phase-contrast effect. The beam produced by the ID19 W150 wiggler at a gap of 59mm
126 was filtred by 2.8mm of aluminium and 1.4mm of copper, resulting in an average detected energy of
127 77.4 keV. The scintillator was a 2000-µm-thick LuAG:Ce (lutetium–aluminium–garnet) crystal. The
128 detector was a PCO edge 4.2 sCMOS. The final reconstruction (46.68µm) was obtained after binning
129 with the software ImageJ.

130   Stage 3 – Pup 2 (with yolk sac resorbed) (CCC 162.21)

131 The specimen was scanned using long propagation phase-contrast synchrotron X-ray
132 microtomography at the ID19 beamline of the European Synchrotron Radiation Facility (ESRF),
133 Grenoble (France). It was scanned at a voxel size of 30.45 µm using the ID19 W150 wiggler at a gap of
134 50mm filtered by 2mm of aluminium, 0.25mm of copper and 0.25mm of tungsten. The scintillator,
135 detector and distance between the sample and the detector were the same as for fetus. The final
136 reconstruction (60.90µm) was obtained after binning in ImageJ.

137   Stage 4 – Juvenile (CCC 94)

138 The specimen was scanned twice, once at the ESRF (Grenoble, France) and once using an MRI scan at
139 the ICM (Paris, France). At the ESRF, the specimen was scanned at a voxel size of 28.43 µm and using
140 a propagation distance of 13m to maximize the phase-contrast effect. The beam produced by the
141 ID19 W150 wiggler at a gap of 30mm was filtered by 2mm of aluminium and 15mm of copper, resulting

142 in an average detected energy of 170 keV with a bandwidth of 85 keV FWHM. The detector camera

143 was a FreLoN 2K charge coupled device mounted on a lens system composed of a 750-mm-thick

144 LuAG:Ce scintillator. The final reconstruction (56.86 µm) was obtained after binning in ImageJ, and

145 used for the 3D-rendering of the pectoral girdle. As the contrast was not excellent, possibly due to a

146 historical treatment by injection of a colloidale baryte solution (Anthony, 1980), the specimen was re-

147 scanned in MRI at the Centre for NeuroImaging Research, ICM (Brain & Spine Institute). MRI was

148 performed at 3T with a Siemens Tim TRIO (Siemens, Germany) system. Images were acquired with a

149 3D Flash sequence with an isotropic resolution of 300 µm. Parameters were: Matrix size =

150 640*300*256; TR/TE (ms) = 18/4.73; Flip Angle = 10°; Spectral Width = 100 kHz; Number of averages

151 = 20; Total acquisition time was 7 hours and 41 minutes. The RMI data were used for the 3D-rendering

152 of the pectoral fin endoskeleton.

153 Synchrotron data were reconstructed using a filtered back-projection algorithm coupled with a single

154 distance phase-retrieval process (Paganin *et al.*, 2002; Sanchez *et al.*, 2012). For each sample, all the

155 sub-scans were reconstructed separately, converted into 16-bit TIFF stacks and then concatenated to

156 generate a single complete scan of each specimen. The ring artefacts were corrected on the

157 reconstructed slices using a specific tool developed at the European Synchrotron Radiation Facility

158 (Lyckegaard *et al.*, 2011).

159   Stage 5 – Adult (CCC 22)

160 The specimen CCC 22 was scanned with a high-resolution computerized axial tomography scanning

161 (CAT scan) in a Parisian Hospital (France) using the following scanning parameters: effective energy

162 120 kV, current 158 mA, voxel size 742 µm and 1,807 views.

163 The slices were reconstructed and exported into 16-bit TIFF stacks using the phoenix datos|x 2.0

164 reconstruction software, and exported into 16-bit TIFF stacks.

165 *Segmentation and 3D-reconstruction method*

166 For all the specimens, segmentation and three-dimensional rendering were done using the software

167 MIMICS Innovation Suite 20.0 (Materialise).

168 **Results** :

169 *The pectoral girdle*

170 In the adult, the pectoral girdle is composed of four flattened and elongated dermal bones – the

171 clavicle, the cleithrum, the anocleithrum and the extracleithrum – and one endochondral bone, the

172 scapulocoracoid as described by Millot & Anthony (1958) (Fig. 2). The girdle forms an arc posterior to

173   the branchial arches. Since the general morphlogy of the pectoral girdle does not change between the

174   different stages, our illustrations depict pup 2 only (Fig. 2).

175   The pectoral girdle is already well developed in the fetus, and does not change dramatically in the four

176   successive stages (Fig. 3). Indeed, the bones continue to grow, but conserve their general shape.

177   However, there is a shift in orientation of the complete pectoral complex (Fig. 4) between the fetus

178   and pup 1. In the fetus, the medial margins of the girdles are oriented toward the ventral side of the

179   embryo, there is no contact between the anterior part of the girdles, and the extracleithrum has a

180   dorsal position on the scapulocoracoid. In pup 1, the medial margins of the girdles rotate in a dorsal

181   direction, leading to the contact between their two anterior extremities, also observed in the following

182   stages, and the extracleithrum has a more lateral position on the scapulocoracoid (Fig. 4). In the

183   juvenile the cleithrum, extracleithrum and clavicle of the pectoral girdle move progressively in closer

184   contact to one another. In the adult stage, these three bones are in close contact with one another

185   with the edges of the bones overlapping. On the μCT scan the three bones appear fused, yet this may

186   be due to the limited resolution of the scan. Indeed, the observation of isolated pectoral girdles shows

187   that the three bones are not fused and that each bone is independent.

188   • The anocleithrum (ano.)

189   It is the most dorsal bone of the pectoral girdle, closely located, but without contact, to the medial

190   side of the dorsal end of the cleithrum. It is a small flat and straight bone, oriented dorso-ventrally.

191   The anocleithrum is attached to the cleithrum by a ligament, as described previously by Millot &

192   Anthony (1958). The general morphology of this dermal bone changes dramatically during

193   development.

194   In the fetus, the anocleithrum is straight and proportionally smaller compared to other stages (Fig. 3).

195   In lateral view, it extends beyond the antero-dorsal margin of the dorsal end of the cleithrum. In pup

196   1, the anocleithrum is proportionally longer, and gently curved to follow the lateral body surface. It

197   also extends beyond the antero-dorsal margin of the dorsal end of the cleithrum. From pup 2 onwards,

198   it extends beyond both the antero-dorsal and postero-ventral margins of the dorsal end of the

199   cleithrum (Fig. 5).

200   The anocleithrum shows some individual variability and asymmetry. Pup 1 has a right anocleithrum

201   with a convex shape in anterior direction, whereas the left one is straight (Fig. 5 A). In pup 2, the left

202   anocleithrum is S-shaped whereas the right one is straighter (Fig. 5 B). The right anocleithrum of the

203   adult is bifid with a backward pointing process whereas the left one is straight (Fig. 5 D). This condition

204   was previously noticed by Millot & Anthony (1958) in another adult specimen (MNHN AC-2012-1 = CCC

205   3).

7

206 • The cleithrum (cl.)

207 In the adult, the cleithrum is an elongated bone fused with the extracleithrum and the clavicle, and
208 overlapping the dorsal surface of the scapulocoracoid (Fig. 2). The medial margin of the cleithrum
209 forms a gutter to accommodate the medial margin of the scapulocoracoid. The cleithrum contacts the
210 extracleithrum at its lateral edge, and in its posterior part forms a gutter surrounding the lateral margin
211 of the scapulocoracoid until the level of the articular process of the scapulocoracoid. The dorsal part
212 of the cleithrum surrounds the dorsal tip of the scapulocoracoid. The uppermost part of the cleithrum
213 is flattened latero-medially and flared dorso-ventrally, with a more or less pronounced longitudinal
214 ridge on the lateral side of the bone. In the fetus, the dorsal lamina of the cleithrum is dorso-medially
215 oriented. Its dorsal tip is pointed and its anterior margin slightly convex (Fig. 3). In later stages, the
216 dorsal tip is spatula-shaped and the anterior margin tends to be progressively more concave (Fig. 3).

217 • The extracleithrum (ecl.)

218 The extracleithrum has an elongated diamond shape and its lateral margin extends lower than the
219 lateral margin of the scapulocoracoid (Fig. 2). Its postero-medial edge contacts the cleithrum and its
220 antero-medial margin is overlapped by the clavicle. The scapulocoracoid fits in the gutter-shaped
221 internal side of the lateral margin of the extracleithrum (Fig. 2). In the fetus, the lateral margin of the
222 extracleithrum simply follows the lateral margin of the scapulocoracoid. The gutter-type contact
223 present in later stages is not formed yet.

224 The extracleithrum is separated from the clavicle by a gap that decreases during the development and
225 disappears from the juvenile onwards. In pup 1, the lateral margin of the extracleithrum extends
226 beyond the lateral margin of the scapulocoracoid and a long gutter appears on its internal side from
227 pup 2 onwards.

228 • The clavicle (cla.)

229 In the adult, the enlarged posterior part of the clavicle is positioned at the antero-lateral part of the
230 scapulocoracoid (Fig. 2). In cross-section, it appears that the posterior tip of the clavicle overlaps the
231 margins of the cleithrum and extracleithrum (Fig. 6). The medial and lateral margins of the clavicle
232 form two gutters where the lateral angle of the scapulocoracoid fits into, then extends antero-ventrally
233 as a twisted shank (Fig. 2). This shank is horizontal, medially concave and reaches the median plane of
234 the ventral side of the body. According to Millot & Anthony (1958), both twisted shanks articulate with
235 a narrow basal lamina, located at the mid-line, but this basal lamina cannot be observed in the imaging
236 data.

237   In the fetus, the medial and lateral margins of the clavicle do not form a gutter and the clavicle does

238   not totally surround the lateral angle of the scapulocoracoid (Fig. 6A). The posterior part of the clavicle

239   is only in contact with the extracleithrum. There is no contact between the anterior twisted shanks of

240   the right and the left clavicles. From pup 1 onwards, the clavicles are ventrally in contact and form with

241   the scapulocoracoid a hemi-circle and the posterior part of the clavicle partially overlaps the cleithrum

242   (Fig. 6 B-C). In this stage, the lateral margin of the clavicle extends ventrally and begins to form a gutter.

243   In pup 2 and the following stages, the lateral and medial margins of the clavicle form two small gutters

244   that surround the lateral angle of the scapulocoracoid. From pup 2 onwards, the posterior tip of the

245   clavicle overlaps both the margins of the cleithrum and extracleithrum.

246   • The scapulocoracoid (scc.)

247   This massive element is overlapped by the cleithrum, extracleithrum and clavicle (Fig. 2, Fig. 3). It is

248   the only endochondral bone of the pectoral girdle. It is composed of two parts: a long triangular-

249   shaped blade, with a dorsal tip and a ventral base, positioned on the internal side of the cleithrum,

250   and a short and massive articular process for the pectoral fin, posteriorly oriented. The anterior margin

251   of the triangular-shaped blade is concave. The lateral and dorsal angles of the scapulocoracoid are very

252   sharp and respectively surrounded by the the clavicle and the cleithrum (Fig. 2 A). The massive articular

253   process of the scapulocoracoid is posteriorly oriented along the body axis, and round in transverse

254   section. The end of this process is a flat quadrangular surface with a small articular head at the supero-

255   lateral angle. This articular head corresponds to the glenoid process and forms a ball-and-socket joint

256   (Miyake *et al.*, 2016), and articulates with the first endoskeletal element of the fin.

257   In the fetus, the dorsal angle of the scapulocoracoid is rounded and slightly curved towards its outer

258   side (Fig. 3). The dermal elements of the girdle do not lie directly on the triangular part of the

259   scapulocoracoid, but are separated by a large space (Fig. 6 A). The articular process presents four

260   concave faces in transverse section. From pup 1 onwards the dorsal angle is straight and sharp. The

261   dermal bones closely overlap the scapulocoracoid (Fig. 6). The articular process is more robust and

262   large, rounded in transverse section (Fig. 3).

263   *The pectoral fin* (Fig. 7)

264   The pectoral fin of *Latimeria* is composed of different elements: mesomeres on the metapterygial axis,

265   pre-axial elements (corresponding to the pre-axial radials and pre-axial accessory elements), and post-

266   axial elements (corresponding to the post-axial accessory elements and the distal radial) (Fig. 7).

267   According to Millot & Anthony (1958), the metapterygial axis of the fin consists of five axial elements,

268   named "*articles*" and numbered from proximal to distal. However, Ahlberg (1989) identified four

269   mesomeres and one distal radial element. There are four pre-axial radial elements (Millot & Anthony,

270 1958; Forey 1998), a variable number of pre-axial and post-axial accessory elements (Millot & Anthony,

271 1958) (Fig. 7). The fin rays insert on the pre- and post-axial accessory elements, on the fourth pre-axial

272 radial and on the distal radial (Fig. 7). According to Millot & Anthony (1958), the fifth axial element is

273 different in shape from the first to fourth ones, and the fin rays articulate at its distal edge, whereas

274 the previous axial elements do not articulate with the fin rays. In this regard, and following Forey

275 (1998), we here refer to four mesomeres on the metapterygial axis and one distal radial that belongs

276 to the post-axial elements. The term of "mesomeres" is used after Jarvik (1980) as the subcylindrical

277 radial segments of the principal axis in sarcopterygian fins.

278 According to Johanson *et al.* (2007), the three first axial elements are homologous to the humerus,

279 ulna and ulnare of tetrapodomorphs and tetrapods. Similarly, the two first pre-axial radial elements

280 are considered homologous to the radius and intermedium of tetrapods (Johanson *et al.*, 2007). The

281 reference position of the pectoral fin is with the fin positioned along the body, its leading edge oriented

282 dorsally. This position corresponds to the position of the pectoral fin of embryos within the oviduct

283 (Forey, 1998).

284 1) The metapterygial axis

285 The first and second mesomeres (Forey, 1998) have a similar quadrangular prismatic shape with

286 slightly concave faces, as described by Millot & Anthony (1958). The dorsal and ventral edges ("*bord*

287 *supérieur*" and "*bord inférieur*" cfr. Millot & Anthony, 1958) of the first mesomere form both a ridge

288 directed from the proximal to the distal side. The dorsal ridge is well developed and extends further

289 than the distal end of the bone. The distal part of the ridge is directed to the medial plane ("*interne*"

290 for Millot & Anthony), when the fin is in resting position. The ventral ridge is also well developed and

291 has a hook ("*crochet*" for Millot & Anthony) directed towards the medial plane (Fig. 7, Supplementary

292 Fig. 1). The lateral and medial edge ("*externe*" and "*interne*" edge for Millot & Anthony, 1958) of the

293 mesomeres are angular but smooth and they do not form a ridge (Supplementary Fig. 1).

294 Each mesomere is longer than wide and presents a proximal joint ("*extrémité antérieure*" for Millot &

295 Anthony, 1958) that is concave and a distal joint convex ("*extrémité postérieure*" for Millot & Anthony,

296 1958).

297 • The first mesomere (mes. 1)

298 This mesomere has the same orientation in our virtual dissection as described by Millot & Anthony

299 (1958) and we can define the four facets: the dorso-medial, the dorso-lateral, the ventro-lateral and

300 ventro-medial ("*supéro-interne*", "*supéro-externe*", "*inféro-externe*" and "*inféro-interne*" for Millot &

301 Anthony, 1958) (Supplementary Fig. 1). It is the largest mesomere of the fin.

302   In the fetus, the transverse section of this mesomere shows four highly concave facets (Fig. 9 A). The

303   joint with the scapulocoracoid (called glenoid surface by Millot & Anthony, 1958) is also concave, and

304   located on the lateral side of the mesomere, extending proximally (Fig. 8, Fig. 9 C, D). The dorsal and

305   ventral ridges of the first mesomere are slightly oblique to the medial plane at the distal end of the

306   mesomere. These ridges begin at the level of the joint with the scapulocoracoid and end at the distal

307   part of the first mesomere. From pup 1 onwards, the first mesomere is fully formed and presents a

308   quadrangular prismatic shape. Its cross section shows that its facets are less concave than in fetus (Fig.

309   9 B). The articular surface with the head of the scapulocoracoid is highly concave. As in the following

310   stages, it is mainly located on the lateral side of the mesomere with only a lateral swollen margin

311   (Supplementary Fig. 1). From pup 1 to the adult, the morphology of the first mesomere does not

312   change (except in size). In these stages, we can observe an asymmetry between the right and left side.

313   The left mesomere has a double hook that forms the beginning of a loop (Fig. 9 E), whereas the right

314   mesomere has only a single hook (Fig. 9 F).

315   • The second mesomere (mes. 2)

316   This mesomere is smaller than the first one. As described by Millot & Anthony (1958), its proximal joint

317   is less concave than that of the first mesomere. Despite a similar morphology as the first mesomere,

318   its orientation is different and the bone shows a rotation around the fin axis (Supplementary Fig. 1).

319   The dorsolateral face of the mesomere 1 corresponds to the dorsal face of the mesomere 2, the

320   ventrolateral face corresponds to the lateral face, the ventromedial face to the ventral face and the

321   dorsomedial face to the medial face (Supplementary Fig. 1). The proximal joint of this mesomere is not

322   in lateral position as in the first mesomere, but it covers the proximal surface (Supplementary Fig. 1).

323   This joint surface is less deep compared to the first mesomere and a peripheral swollen edge surrounds

324   it, whereas the first mesomere has only a lateral swollen edge around the proximal joint

325   (Supplementary Fig. 1). In fetus, its morphology is similar to that of the first mesomere: longer than

326   wide, thin, and with highly concaves faces (Fig. 9 C, D). In this stage, it is not clear that there is a rotation

327   of the elements along the metapterygial axis. From pup 1 onwards, it is fully formed with a

328   quadrangular prismatic shape and concave faces. As for the first mesomere, the second mesomere

329   shows some asymmetry. In pup 2, the ventrolateral ridge of the right fin wears a double hook that

330   forms a loop (Fig. 9 G), whereas on the left fin, the second mesomere only has a single hook (Fig. 8,

331   Fig. 9 H).

332   • The third mesomere (mes. 3)

333   As for the second mesomere, this element shows a rotation around the axis of the fin. Here, the dorsal

334   face of the second mesomere corresponds to the dorsomedial face, the lateral face corresponds to the

335 dorsolateral face, the ventral face to the ventrolateral face and the medial face to the ventromedial

336 face. Therefore, the dorsal edge of the first mesomere corresponds to the medial edge of this

337 mesomere and the dorsolateral face of the first mesomere corresponds to the dorsomedial face. This

338 mesomere is more transversely flattened than the previous one. The dorsal and ventral ridges of the

339 first mesomere corresponds to the medial and lateral ridges. As for the previous mesomere, the ridges

340 are on the medial and lateral edge of the third mesomere (corresponding to the dorsal and ventral

341 edge of the first mesomere) separating the dorsomedial and ventromedial faces (and dorsolateral and

342 ventrolateral faces) of the mesomere. These two ridges, directed from the proximal to distal, present

343 the same shape. The proximal first third is oblique and slopes down to the ventral side. The distal two-

344 thirds slope slightly up until the distal extremity of the mesomere (Fig. 10 C-F). The lateral ridge does

345 not present a hook, unlike the ventral ridge of the first mesomere and the ventro-lateral ridge of the

346 second mesomere. The concave proximal joint is less deep than that of the previous mesomere. The

347 distal end of this mesomere is highly convex and articulates with the fourth mesomere and the third

348 pre-axial radial. In the fetus, its morphology is similar to previous mesomeres. From pup 1 onwards, it

349 is fully formed, and its morphology does not change until adult stage (Fig. 8, Fig. 10).

350   • The fourth mesomere (mes. 4)

351 It is the smallest mesomere of the fin. It has the same orientation as the third mesomere and it has the

352 same transverse flattening. Its ventral edge forms a large ridge whereas its dorsal edge is flat (Fig. 7,

353 Fig. 10). The lateral and medial edge of the fourth mesomere form a large bulge and there is a small

354 oblique ridge on the proximal part of the medial edge. This mesomere is surrounded by the third pre-

355 axial radial element at its dorsal edge and by the post-axial accessory elements at its ventral edge (Fig.

356 7, Fig. 10). In the fetus, as for the previous elements, the fourth mesomere is thin, with its faces highly

357 concave in transverse cross section. The ventral edge shows a small ridge, smaller than in the next

358 stages (Fig. 10 A, B). The dorsal edge of the fourth mesomere forms a massive ridge. The lateral and

359 medial edge of the mesomere form each a thin ridge directed from proximal to distal. The medial thin

360 ridge follows the proximo-distal midline along the medial face of mesomere and the lateral ridge is

361 located more ventrally on the fourth mesomere. From pup 1 onwards, it is fully formed and its

362 morphology does not change until the adult stage (Fig. 8, Fig. 10 C-F). The dorsal edge no longer has

363 its triangular shape and becomes flat. The lateral and medial ridges of the fetus now form a bulge

364 directed from proximal to distal and it is more difficult to distinguish the dorsolateral and ventrolateral

365 faces on the lateral side of the mesomere (and the dorsomedial and ventromedial faces from the

366 medial side of the mesomere) (Fig. 10 C-F).

367 2) The pre-axial elements

368   The pre-axial radial elements are located on the dorsal side of the fin (corresponding to the pre-axial

369   side of the fin/limb of most sarcopterygians; Forey, 1998), near to the joint between the mesomeres

370   of the fin. The first and second pre-axial radials have a different morphology from the third and fourth

371   pre-axial radials (Millot & Anthony, 1958). The two first pre-axial radials have an egg-like shape

372   whereas the others are thin and elongated.

373   • The first pre-axial radial (pr. rad. 1)

374   It is positioned at the distal part of the lateral edge of the first mesomere (pre-axial edge), near the

375   joint with the second mesomere. It is slightly shifted towards the dorsolateral face of the first

376   mesomere (Fig. 7, Fig. 8, Fig. 9). It is egg-shaped and slightly thinner on the proximal side. In the fetus,

377   this radial extends to the proximal part of the second mesomere and the distal part of the first

378   mesomere (Fig. 9 C, D), but from pup 1 onwards, it only covers the first mesomere (Fig. 9 E-H). The

379   right and left first pre-axial radials present a different shape. Whereas the right element already shows

380   its ovoid shape, the left element is thinner in transverse section and elongated and extends to the

381   second mesomere more broadly.

382   • The second pre-axial radial (pr. rad. 2)

383   It covers the distal part of the dorsolateral edge of the second mesomere, near the joint with the third

384   mesomere. As for the first pre-axial radial, it is slightly shifted towards the dorsal face of the second

385   mesomere and it is egg-shaped (Fig. 7, Fig. 8, Fig. 9). According to Millot & Anthony (1958), this element

386   is thinner and more elongated than the first pre-axial radial. However, our segmentation and the

387   different isolated pectoral fins of adult specimens (CCC 6; CCC 7; CCC 14; CCC 19) show a similar size

388   and shape of the two elements. In the fetus, this second pre-axial radial is elongated and thin in

389   transverse section and covers the proximal part of the third mesomere (Fig. 8, Fig. 9 C, D). From pup 1

390   onwards, the second pre-axial radial is less elongated and egg-shaped, and covers only the distal part

391   of the second mesomere (Fig. 8, Fig. 9 E-H).

392   • The third pre-axial radial (pr. rad. 3)

393   This radial differs from the previous radials in shape. It is thin and elongated, oval-shaped, and taller

394   than the fourth mesomere that it covers (Fig. 7). At its distal end, there is a small pointed element,

395   which is the tip of the third pre-axial radial. This element carries fin rays 25 to 28 (Fig. 7). The proximal

396   part of this element is straight and it articulates with the third mesomere. In the fetus, it could only be

397   segmented for the right fin. This element is closely associated with the fourth pre-axial radial and the

398   pre-axial accessory elements and is part of a large cartilaginous plate (Fig. 10 A, B). In pup 1, the

399   cartilaginous plate is segmented and the third pre-axial radial is differentiated from the fourth pre-

13

400   axial radial and the pre-axial accessory elements (Fig. 10). From pup 1 onwards, the third pre-axial

401   radial presents its elongated oval shape and has a small separated tip.

402   • The fourth pre-axial radial (pr. rad. 4)

403   This element is positioned at the distal end of the fin endoskeleton in association with the distal radial.

404   As for the third pre-axial radial, this element is elongated and thin, but it has a trapezoidal shape with

405   three straight edges and one curved edge (Fig. 7, Fig. 10). The ventral straight edge is in contact with

406   the distal radial and its dorsal edge is in contact with the third pre-axial radial and its tip. It articulates

407   with distal part of the fourth mesomere by its proximal straight edge (Fig. 10). Its distal edge is curved

408   and carries fin rays 20 to 24 (Fig. 7). In the fetus it appears that the third pre-axial radial and the fourth

409   pre-axial radial form a unique cartilaginous plate that covers at least the fourth mesomere and the

410   distal radial in the left fin (Fig. 10 A) and also the third mesomere in the right fin (Fig. 10 B). Between

411   the fetus stage and the pup 1 stage, this element becomes segmented into several elements: the third

412   pre-axial radial with its pre-axial accessory elements and its tip, and the fourth pre-axial radial

413   described just above (Fig. 8, Fig. 10). From pup 1 onwards, the fourth pre-axial radial presents its

414   trapezoidal shape (Fig. 10 C-F).

415   • Pre-axial accessory elements (pr. acc.)

416   These elements (called "*éléments accessoires de la troisième pièce radiale préaxiale*" by Millot &

417   Anthony, 1958) are positioned at the dorsal edge of the third mesomere and associated to the third

418   pre-axial radial. There is one large element in contact with the third mesomere, one large element in

419   contact with both the third mesomere and the previous element that carries the fin rays 31 and 32,

420   and one large element in contact with the third mesomere and the third pre-axial radial that carries

421   the fin rays 29 and 30 (Fig. 7). There are also several smaller elements, between two and four, in

422   contact with the larger elements or with the third pre-axial radial, but their number varies depending

423   on the development stage (Fig. 7, Fig. 8, Fig. 10). In the fetus, there are no differentiated pre-axial

424   accessory elements. These elements belong to the same large cartilaginous plate as the third pre-axial

425   radial and the fourth pre-axial radial (Fig. 10 A, B). From pup 1 onwards, the cartilaginous plate

426   becomes segmented in several elements and the pre-axial accessory elements are differentiated from

427   the third pre-axial radial and the fourth pre-axial radial (Fig. 10). It seems that the number of pre-axial

428   accessory elements is not fixed and can differ between the right and left fins within an individual (Fig.

429   7). In pup 1, there are six elements on the right fin with three small elements, whereas there are seven

430   elements on the left fin with four small elements. In pup 2, there is the same organization with three

431   small pre-axial accessory elements of the right fin, but only two small elements on the left fin

432   (associated with the three large elements). In the adult, Millot & Anthony (1958) described seven

433   elements on the pre-axial accessory elements, three large elements and four small elements. Our 3D

434   segmentation shows only one large cartilaginous element identified by µCT, but the different isolated

435   pectoral fin skeletons show seven elements, as described by Millot & Anthony (1958).

436   3)   The post-axial elements

437   • The distal radial (dis. rad.) (Fig. 7)

438   As described by Millot & Anthony (1958), this element is transversely flattened and it has an elongated

439   trapezoid shape. Its shape is similar to the fourth pre-axial radial and it is its symmetric, but slightly

440   taller (Fig. 7, Fig. 10). It has three straight edges and one curved convex edge. In transverse section the

441   distal radial present two slightly convex faces (Supplementary Fig. 2). Its dorsal straight edge is aligned

442   with the proximo-distal axis of the fourth mesomere and it is close to the fourth pre-axial radial

443   element. The proximal joint is straight. Its ventral edge is straight and in contact with the distal post-

444   axial accessory element. The curved edge is positioned at the distal part of the ventral edge of this

445   element. It is on this edge that the fin rays 11 to 19 are inserted (Fig. 7). In the fetus, the distal radial

446   already presents a shape similar to that observed in the adult. It is transversely flattened, but presents

447   a lateral ridge directed from proximal to distal (Fig. 10 A, B). In pup 1, there is no lateral ridge on this

448   element (Fig. 10 C, D). From pup 2 onwards, there is a small swelling on its dorsal edge. This swelling

449   is triangular shaped, as wide as its edge on the proximal part, then decreasing in size (Fig. 10 E, F).

450   • The post-axial accessory elements (po. acc.)

451   According to Millot & Anthony (1958), there are five post-axial accessory elements in the adult stage.

452   However, in the different isolated pectoral fins of adult specimens observed (CCC 6; CCC 7; CCC 14;

453   CCC 19), we can see only four elements, aligned along the ventral ridge of the fourth mesomere. The

454   proximal and the distal post-axial accessory elements are the largest ones and have a similar shape.

455   The proximal element articulates with the proximal part of the ventral edge of the fourth mesomere.

456   It is triangular-shaped with the tip directed to the proximal side of the fin and leaves a large gap

457   between this element and the third mesomere (Fig. 7, Fig. 8. Fig. 10). The second and third post-axial

458   accessory elements are small and globular. The distal element is similar to the first element. This

459   element is in contact with the distal part of the ventral edge of the fourth mesomere and the ventral

460   edge of the distal radial. The first ten fin rays insert on the ventral edge of these post-axial accessory

461   elements: 1 to 5 on the first element, ray 6 on the second element, ray 7 on the third, and rays 8 to 10

462   on the fourth element (Fig. 7). In the fetus, there is only one large post-axial accessory element

463   identified in the µCT (Fig. 10 B). This element is in contact with the fourth mesomere and the proximal

464   part of the ventral edge of the distal radial. It appears segmented at pup 1 and pup 2, as for the pre-

465   axial cartilaginous plate. In pup 1, we can observe an asymmetry between the right and left fin for

466   these elements. In the right fin, the elements are as described above, but in the left fin, the third

467   element is slightly different, being flat and trapezoidal-shaped (Fig. 10 C). In pup 2, there is no

468   asymmetry between the right and left pectoral fins for these elements. In the juvenile and adult, the

469   µCT data do not allow us to identify more than one small element (Fig. 8).

470   4) The fin rays

471   There are 32 fin rays on the pectoral fin. There are numbered 1 to 32 from the ventral side to the dorsal

472   side (Fig. 7). As described by Millot & Anthony (1958) the proximal part of the fin ray is bifurcated, and

473   one branch inserts on the lateral side of the fin and the other on the medial side. The first ray is very

474   small and the next becomes longer until ray 20 after which the length of the fin rays decreases. The

475   fins rays of the pre-axial side of the fin insert largely on the pre-axial radials elements: rays 29 to 32

476   insert on the pre-axial accessory elements, rays 25 to 28 insert on the third pre-axial radial, and rays

477   20 to 24 insert on the curved edge of the fourth pre-axial radial. On the post-axial side of the fin, the

478   fin rays insert only on the edge of the elements: the fin rays 11 to 19 on the curved edge of the distal

479   radial and rays 1 to 10 on the edge of the post-axial accessory elements. In the fetus, the fin web is

480   rounded and there seems to be no clear leading edge. From pup 1 onwards, the fin web has the same

481   morphology as in the adult, forming a fin web that is elongated and pointed, with a convex leading

482   edge and a concave trailing edge.

483   **Discussion**

484   As the period of gestation remain unknown in the extant coelacanths, it was consequently not possible

485   to establish precise relationships between the known ontogenetic stages in vertebrates and those

486   described here for *Latimeria*. We have gathered five clearly different ontogenetic stages: three

487   prenatal stages, one juvenile and one adult.

488   *The pectoral girdle*

489   The pectoral girdle shows different arrangements within the different vertebrate groups, with various

490   types of relations between the dermal and endoskeletal elements in relation to the mode of

491   locomotion (McGonnell, 2001). The dermal anocleithrum (in sarcopterygians) or postcleithrum (in

492   actinopterygians), cleithrum and clavicle are primitively present in all osteichthyans (Gosline, 1977;

493   Friedman & Brazeau, 2010; Zhu *et al.*, 2012a). The majority of osteichthyans also has a supracleithrum

494   and/or a post-temporal, both small elements located in the most dorsal part of the girdle as in early

495   tetrapodomorphs (Coates & Ruta, 2007; Friedman & Brazeau, 2010). Coelacanths have the

496   anocleithrum, cleithrum and clavicle in common with the other osteichthyans, but also a

497   supernumerary dermal bone, the extracleithrum, which is considered as a synapomorphy of the group

498 (Forey, 1998). The endoskeletal element of the pectoral girdle, the scapulocoracoid, is present in all

499 vertebrates and is covered by the cleithrum and clavicle in osteichthyans (McGonnell, 2001). In

500 osteichthyan fishes, the scapulocoracoid is usually small compared to other elements of the pectoral

501 girdle and the cleithrum forms a large part of the girdle (Janvier, 1996; McGonnell, 2001; Zhu &

502 Schultze, 2001). However, in *Latimeria chalumnae* the scapulocoracoid is proportionally massive (Figs.

503 3, 5) and is, together with the cleithrum, the largest element of the girdle. A large scapulocoracoid is

504 also present in the lungfish *Neoceratodus forsteri* (Rosen *et al.*, 1981; Johanson *et al.*, 2004) and

505 considered convergent with coelacanths by Coates and Ruta (2007). Within tetrapodomorphs, there is

506 an evolutionary trend towards a reduction of the dermal part of the girdle (clavicle, cleithrum) while

507 the endochondral scapulocoracoid becomes the main component of the girdle in tetrapods

508 (McGonnell, 2001; Vickaryous & Hall, 2006). The presence of a large scapulocoracoid or scapula +

509 coracoid in tetrapods and in the coelacanth *Latimeria* is also considered convergent. Indeed, early

510 tetrapodomorphs as *Eusthenopteron* (Andrews & Westoll, 1970) have proportionally small

511 scapulocoracoids, as for extinct coelacanths as observed in the Triassic coelacanth *Laugia groenlandica*

512 (Stensiö, 1932; Millot & Anthony, 1958) and the Devonian coelacanth *Diplocercides* (Stensiö, 1922).

513 However, it is necessary to be careful with this assumption. Indeed, unlike the dermal elements of the

514 girdle, the coelacanth scapulocoracoid is largely cartilaginous and it is consequently possible that only

515 the most ossified part of this element is preserved in fossils (Forey, 1998). According to Forey (1981),

516 the scapulocoracoid of the Carboniferous coelacanth *Rhabdoderma* was probably more substantial

517 than the preserved mineralized portion, and fit into the groove present in the internal face of the

518 cleithrum as observed in *Latimeria*. If this assumption is correct, the presence of groove on the internal

519 side of dermal bones of the girdle in fossil coelacanths, as in *Diplurus* (Schaeffer, 1952), *Rhabdoderma*

520 (Forey, 1981) or *Trachymetopon* (Dutel *et al.*, 2015), delimit the lateral expansion of the

521 scapulocoracoid.

522 In most osteichthyans the pectoral girdle is formed early in development before the fins or limbs. The

523 cleithrum and clavicle are dermal bones and are known to be the first to appear, the scapulocoracoid

524 appearing later in the development of actinopterygians (Jollie, 1980; Faustino & Power, 1999;

525 Koumoundouros *et al.*, 2001) and of the lungfish *Neoceratodus* (Johanson *et al.*, 2004; Joss & Johanson,

526 2007). In *Latimeria chalumnae*, our observations suggest a similar development since all the elements

527 of the pectoral girdle are present in the fetus. Yet the scapulocoracoid seems deflated and is not in

528 tight contact with the dermal bones (Figs. 3, Fig. 6). Later in development an expected radially outward

529 growth of the scapulocoracoid leads to the close overlapping of the scapulocoracoid by the cleithrum,

530 the extracleithrum and the clavicle, as observed from pup 1 onwards (Fig. 6). These observations let

531 us assume that the scapulocoracoid is formed later in the development than the dermal bones in

532   *Latimeria* as in most vertebrates. The scapulocoracoid consists of a single massive element (Millot &

533   Anthony, 1958) in the early development of the pectoral girdle. This development of the

534   scapulocoracoid of *Latimeria* agrees with Schaeffer's (1941) observation of a complete co-ossification

535   of the scapular and coracoid elements of the girdle for *Undina* and *Macropoma*. However, the

536   development of the endoskeletal bone of the pectoral girdle is different from the actinopterygians.

537   Indeed, in actinopterygians (except for acipenseriforms (Jollie, 1980; Davis *et al.*, 2004)), there are two

538   ossifications regions inside the cartilaginous scapulocoracoid plate that correspond to the scapular and

539   coracoid regions of the girdle (Patterson, 1982; Cubbage & Mabee, 1996; Grandel & Schulte-Merker,

540   1998). In *Neoceratodus*, as for *Latimeria*, there are no distinct ossification centers for the scapular and

541   coracoid regions inside the scapulocoracoid. However, unlike the coelacanth, these two regions are

542   distinct in the adult lungfish and are not co-ossified (Johanson *et al.*, 2004).

543   The anocleithrum is the element of the girdle that proportionally grows the most during development

544   despite remaining the smallest bone of the girdle at the adult stage (Fig. 3). The small and rod-like

545   anocleithrum in *Latimeria* is different in size and proportion from anocleithra known in other

546   sarcopterygian fishes such as *Neoceratodus* or tetrapodomorph fishes (Coates & Ruta, 2007). The

547   anocleithrum of *Latimeria* provides an insertion for the large *levator externus 5* muscle of the branchial

548   arches musculature (Millot & Anthony, 1958; Forey, 1998; Carvalho *et al.*, 2013), likely similar to

549   *Neoceratodus* (Carvalho *et al.*, 2013). However, the homology between the anocleithrum bones of

550   different sarcopterygians has been previously challenged (Campbell *et al.*, 2006) and remains to be

551   validated.

552   In the early stages of development there is a reorientation of the pectoral girdle inside the body. The

553   reorientation of bones during development has been shown in several groups of vertebrates. It is well

554   documented for the pelvic girdle in lissamphibians (Rocková & Rocek, 2005; Pomikal *et al.*, 2011;

555   Manzano *et al.*, 2013), the chicken (Nowlan & Sharpe, 2014) and in mice (Pomikal & Streicher, 2010),

556   and for the pectoral girdle in chelonians (Nagashima *et al.*, 2007). However, the mechanisms of

557   rotation and reorientation of the girdles remain largely unknown. As for the reorientation of the digits

558   during the development in some birds (Botelho *et al.*, 2014), the reorientation of the pectoral girdle in

559   *Latimeria* is probably tightly linked to its interactions with the development of the adjacent muscles.

560   *The pectoral fin*

561   The endoskeletal elements of the pectoral fin known in adult stage are already present in the fetus,

562   except the pre-axial accessory elements and the pre-axial radial elements 3 and 4. The axial elements

563   of the pectoral fin, like the scapulocoracoid, seem deflated in the fetus, and their development

564   between the fetus and pup 1 suggests a significant process of radially outward growth (Fig. 8). The

18

565 large distal cartilaginous plate in the fetus corresponds to the most distal radial elements (pre-axial

566 radial 3 and 4, pre-axial accessory elements) in pup 1. The post-axial accessory elements show a similar

567 development with the post-axial cartilaginous plate in the fetus corresponding to four post-axial

568 accessory elements in pup 1 (Fig. 8). Millot & Anthony (1958) already proposed the fragmentation of

569 a unique cartilaginous plate to form the radial elements. Observations made on the earliest stage

570 confirm the presence of non-differentiated large plates and support this hypothesis. Moreover, in the

571 fetus, the cartilaginous plate articulates with the third and fourth mesomeres and the distal radial,

572 suggesting a positional homology to the pre-axial accessory elements and the pre-axial radial 3 and 4,

573 since these elements are respectively articulated with the third and fourth mesomeres and the distal

574 radial in the later stages of development (Fig. 8; Fig. 10).

575 This splitting of a single endochondral plate to form the elements of the fin is also known in some other

576 groups of vertebrates. This mechanism has been observed in actinopterygians such as *Polyodon* (Davis

577 *et al.*, 2004; Mabee & Noordsy, 2004), the zebrafish *Danio rerio*, the bichir *Polypterus senegalus*

578 (Grandel & Schulte-Merker, 1998), the sturgeon *Acipenser* (Davis *et al.*, 2004). The splitting of the

579 endoskeleton of the fin is made by a decomposition of the extracellular matrix of the endoskeletal

580 plate leading to the formation of the proximal radials (pro- and mesopterygium) (Davis *et al.*, 2004;

581 Nakamura *et al.*, 2016). The primitive condition of the pectoral fin of sarcopterygians is thought to be

582 polybasal with pro-, meso- and metapterygium, as in actinopterygians (Zhu & Yu, 2009). However,

583 crown sarcopterygians, including coelacanths, have lost their pro- and mesopterygium and only retain

584 the metapterygium leading to the mono-basal condition of the fin (Rosen *et al.*, 1981; Janvier, 1996;

585 Zhu & Yu, 2009). In the acipenseriforms *Acipenser* and *Polyodon*, the metapterygial elements are

586 formed outside the endoskeletal plate as an extension of the scapulocoracoid (Davis *et al.*, 2004;

587 Mabee & Noordsy, 2004). These elements are formed in a similar way as are the distal radials of the

588 fins of non-tetrapod sarcopterygians and the limbs in tetrapods (Davis *et al.*, 2004), with a

589 condensation of the mesenchyme from proximal to distal (Shubin & Alberch, 1986; Joss & Longhurst,

590 2001).

591 The development of the metapterygial axis in *Latimeria* might result from a process of segmentation

592 as known in other sarcopterygians and in *Polyodon*. However, this process occurs in the earliest stages

593 of the development of the fin or limb, and only for the formation of the different cartilaginous

594 elements of the endoskeletal axis before the ossification of these elements (Shubin & Alberch, 1986;

595 Joss & Longhurst, 2001; Cohn *et al.*, 2002). Due to the reduced ontogenetic series used in this study

596 we cannot confirm a segmentation process since the elements are already formed and only a growth

597 of the separated endoskeletal elements can be observed. For coelacanths, it is then not possible to

598 identify the mechanism involved in the formation of the metapterygial axis or in the splitting of the

599 cartilaginous plate into pre-axial radial elements or post-axial accessory elements. The splitting of the
600 two pre-axial and post-axial cartilaginous plates to form, respectively, the third and fourth pre-axial
601 radials and the pre-axial accessory elements, and the post-axial accessory elements, seems, however,
602 to be different from the decomposition process of the extracellular matrix of the endoskeletal disc to
603 form the radial elements as known in actinopterygians. Indeed, in actinopterygians, it is the
604 precartilaginous plate that splits during development and that forms the different radial elements.
605 However, this splitting occurs before the condensation of the precartilaginous plate (Grandel &
606 Schulte-Merker, 1998; Davis *et al.*, 2004). In *Latimeria*, it appears that the cartilaginous plate is already
607 condensed in the fetus. This is clearly visible on the µCT data and the different elements of the fins
608 have the same contrast than that of other endochondral bones of the body.

609 *Evolution of the pectoral fin morphology in coelacanths and tetrapodomorph fishes*

610 The radials elements of the pectoral fin are asymmetrically organized around the metapterygial axis.
611 Indeed, each mesomere of the fin is associated with a pre-axial element (radial and/or accessory),
612 whereas only the fourth mesomere is associated with radial elements on its post-axial region (distal
613 radial and accessory elements; Fig. 7). However, the general shape of the first and second pre-axial
614 radials, small and rounded, is clearly different from that of the more distal radials which are longer and
615 flattened (Fig. 7), as previously reported (Millot & Anthony, 1958). This difference in shape between
616 the pre-axial radial elements gives lobe-shaped morphology to the pectoral fin of *Latimeria* compared
617 to the fan-shaped fin morphology known in tetrapodomorph fishes. By contrast, the dermal fin rays
618 are arranged almost symmetrically around the main axis of the pectoral fin and they do not insert on
619 the pre-axial radial 1 and 2 (Fig. 7). The asymmetrical condition of the pectoral fin is more pronounced
620 in the early stage of the development. In the fetus, the first and second pre-axial radials, extending on
621 the next mesomere, are proportionally longer than in the following stages (Fig. 8, Fig. 9 C-D), where
622 these elements are small and only associated with one mesomere (Fig. 7, Fig. 8, Fig. 10 E-H). The
623 proportional reduction of the size of the proximal pre-axial radials with respect to the rest of
624 endochondral elements gives a more lobe-shaped aspect to the fin. Developmental data seem
625 corroborate the scenario of an evolution of the pectoral fin towards a lobe-shaped morphology based
626 on rare fossil coelacanth specimens. Indeed, the species *Shoshonia arcopteryx* (Friedman *et al.*, 2007)
627 from the Devonian of the United States, has elongated and flattened radials on the pre-axial side of
628 the fin. The most proximal pre-axial radials are elongated in *Shoshonia* and are different from the short
629 and rounded first and second pre-axial radials in adult *Latimeria*, providing a more fan-shaped
630 morphology to the fin. Interestingly, the earliest stage of *Latimeria* also presents elongated proximal
631 pre-axial radials. As seen in *Latimeria* since the fetus stage, only the distal mesomere is associated with
632 a post-axial radial. The fin rays of *Shoshonia* are associated with all the pre-axial radials, which gives

633   the fin a more asymmetrical profile of the fin web (Friedman *et al.*, 2007). This asymmetrical

634   disposition of the fin rays is also observed in other fossil coelacanths (Forey, 1998; Friedman *et al.*,

635   2007) including *Laugia groenlandica* (Stensiö, 1932) from the Triassic of Greenland. The condition

636   observed in these fossils is thus different from the near-symmetrical arrangement of the fin rays in

637   *Latimeria*. An asymmetrical arrangement of the radial elements and fin rays along the metapterygial

638   axis is also observed in tetrapodomorph fishes (Andrews & Westoll, 1970; Shubin *et al.*, 2006; Friedman

639   *et al.*, 2007), whereas in dipnomorph fishes the pectoral fin is very symmetrical (Ahlberg, 1989;

640   Friedman *et al.*, 2007). The fin rays usually insert on the pre- and post-axial radial elements, except in

641   osteolepiforms where they also insert on the post-axial process of the mesomeres (Friedman *et al.*,

642   2007). According to several authors it is possible that the post-axial process and the post-axial radials

643   have a same ontogenetic origin which could explain the insertion of the fin rays on the mesomere

644   (Jarvik, 1980; Friedman *et al.*, 2007).

645   In contrast, the endochondral elements in the pectoral fin of dipnomorphs are nearly symmetrical with

646   an arrangement of pre-axial and post-axial radials all along the metapterygial axis (Ahlberg, 1989;

647   Friedman *et al.*, 2007; Jude *et al.*, 2014). Yet, the condition observed in lungfish appears to be highly

648   derived with respect to the ancestral condition of sarcopterygian. The presence of an internally and

649   externally asymmetrical pectoral fin in coelacanths and other lobe-finned fishes suggests that this

650   condition is ancestral for sarcopterygians, as firstly proposed by Ahlberg (1989). This interpretation is

651   supported by our observations made on the development of *Latimeria*. The particular morphology of

652   the pectoral fin in *Latimeria* might be linked to changes in the mobility of the fin and in the locomotion,

653   but this hypothesis remains to be tested.

654   **Conclusion**

655   The bony elements of the girdle and pectoral fin of the extant coelacanth *Latimeria* are nearly fully

656   developed in the earliest stage of the ontogenetic series described here. During the first steps of

657   pectoral fin development there is a re-orientation of the girdle putting the scapulocoracoids and the

658   clavicles in the ventro-medial region of the two girdles in contact. The anocleithrum is the dermal bone

659   of the girdle that proportionally grows the most during the development, further showing considerable

660   morphological plasticity. The scapulocoracoid is robust which is unusual in most osteichthyans with

661   the exception of tetrapods. The earliest developmental stage specimen shows a deflated

662   scapulocoracoid and a lack of contact between the mesomeres and the scapulocoracoid with the

663   dermal bones of the girdle. This early stage specimen also presents two large cartilaginous plates, on

664   pre-axial and post-axial sides of the fin that later split into the pre-axial accessory elements and the

665   third and fourth pre-axial radial, and in the post-axial accessory elements. The internal shape of the

666   pectoral fin further becomes progressively more lobe-shaped due to a proportional reduction of the

667   proximal pre-axial radials during development. Our developmental data corroborate previous fossil

668   evidence, and reinforce the hypothesis that the lobe-shaped pectoral fin in the living coelacanth

669   derives from the primitive fan-shaped condition of sarcopterygians.

Abbreviations

671   ano., anocleithrum; cl., cleithrum; cla., clavicle; dis. rad., distal radial; ecl., extracleithrum; f. r., fin ray;

672   mes., mesomere; po. acc., post-axial accessory elements; pr. acc., pre-axial accessory elements; pr.

673   rad., pre-axial radial; scc., scapulocoracoid

Data Availability Statement

685   All the data are available by request from the authors.

References

693   **Ahlberg PE** (1989) Paired fin skeletons and relationships of the fossil group Porolepiformes

694   (Osteichthyes: Sarcopterygii). *Zool. J. Linn. Soc.* **96**, 119–166.

695   **Ahlberg PE** (1991) A re-examination of sarcopterygian interrelationships, with special reference to

696   the Porolepiformes. *Zool. J. Linn. Soc.* **103**, 241–287.

697   **Amaral DB, Schneider I** (2017) Fins into limbs: Recent insights from sarcopterygian fish. *Genesis* **56**,
698   1–8.

699   **Amemiya CT, Alfoldi J, Lee AP,** *et al.* (2013) The African coelacanth genome provides insights into
700   tetrapod evolution. *Nature* **496**, 311–316.

701   **Andrews SM, Westoll TS** (1970) The Postcranial Skeleton of *Eusthenopteron foordi* Whiteaves.
702   *Earth Environ. Sci. Trans. R. Soc. Edinburgh* **68**, 207–329.

703   **Anthony J** (1980) Evocation des travaux français sur *Latimeria* notamment depuis 1972. *Proc. R.*
704   *Soc. B Biol. Sci.* **208**, 349–367.

705   **Botelho JF, Smith-Paredes D, Nuñez-Leon D, Soto-Acuña S, Vargas AO** (2014) The developmental
706   origin of zygodactyl feet and its possible loss in the evolution of Passeriformes. *Proc. R. Soc. B*
707   *Biol. Sci.* **281**, 20140765.

708   **Campbell KSW, Barwick RE, den Blaauwen JL** (2006) Structure and function of the shoulder girdle in
709   dipnoans: new material from Dipterus valenciennesi. *Senckenbergiana lethaea* **86**, 77–91.

710   **Carvalho M, Bockmann FA, de Carvalho MR** (2013) Homology of the Fifth Epibranchial and
711   Accessory Elements of the Ceratobranchials among Gnathostomes: Insights from the
712   Development of Ostariophysans. *PLoS One* **8**.

713   **Casane D, Laurenti P** (2013) Why coelacanths are not "living fossils": A review of molecular and
714   morphological data. *BioEssays* **35**, 332–338.

715   **Cavin L, Guinot G** (2014) Coelacanths as 'almost living fossils'. *Front. Ecol. Evol.* **2**, 1–5.

716   **Cavin L, Mennecart B, Obrist C, Costeur L, Furrer H** (2017) Heterochronic evolution explains novel
717   body shape in a Triassic coelacanth from Switzerland. *Sci. Rep.* **7**, 1–7.

718   **Clack JA** (2012) *Gaining Ground: The Origin an Evolution of Tetrapods*. Indiana University Press,
719   Bloomington.

720   **Clack JA** (2009) The Fin to Limb Transition: New Data, Interpretations, and Hypotheses from
721   Paleontology and Developmental Biology. *Annu. Rev. Earth Planet. Sci.* **37**, 163–179.

722   **Coates MI** (2003) The Evolution of Paired Fins. *Theory Biosci.* **122**, 266–287.

723   **Coates MI, Jeffery JE, Ruta M** (2002) Fins to limbs: What the fossils say. *Evol. Dev.* **4**, 390–401.

724   **Coates MI, Ruta M** (2007) Skeletal Changes in the Transition from Fins to Limbs. In: *Fins into Limbs -*

725   *Evolution, Development, and Transformation*, pp. 15–38 The University of Chicago Press,
726   Chicago.

727 **Cohn MJ, Lovejoy CO, Wolpert L, Coates MI** (2002) Branching, segmentation and the metapterygial
728   axis: Pattern versus process in the vertebrate limb. *BioEssays* **24**, 460–465.

729 **Cubbage CC, Mabee PM** (1996) Development of the cranium and paird fins in the zebrafish *Danio*
730   *rerio* (Ostariophysi, Cyprinidae). *J. Morphol.* **229**, 121–160.

731 **Davis MC, Shubin NH, Force A** (2004) Pectoral fin and girdle development in the basal
732   actinopterygians *Polyodon spathula* and *Acipenser transmontanus*. *J. Morphol.* **262**, 608–628.

733 **Dutel H, Galland M, Tafforeau P, *et al.*** (2019) Neurocranial development of the coelacanth and the
734   evolution of the sarcopterygian head. *Nature* **7206**.

735 **Dutel H, Herbin M, Clément G** (2015) First occurrence of a mawsoniid coelacanth in the Early
736   Jurassic of Europe. *J. Vertebr. Paleontol.* **35**, 0–13.

737 **Erdmann M V, Caldwell RL, Moosa MK** (1998) Indonesian 'king of the sea' discovered. *Nature* **395**,
738   335.

739 **Faustino M, Power DM** (1999) Development of the pectoral, pelvic, dorsal and anal fins in cultured
740   sea bream. *J. Fish Biol.* **54**, 1094–1110.

741 **Forey PL** (1998) *History of the Coelacanth Fishes*. Chapman & Hall, London.

742 **Forey PL** (1981) The coelacanth *Rhabdoderma* in the Carboniferous of the British Isles.
743   *Paleontology* **24**, 203–229.

744 **Fricke H, Hissmann K** (1992) Locomotion, fin coordination and body form of the living coelacanth
745   *Latimeria chalumnae*. *Environ. Biol. Fishes* **34**, 329–356.

746 **Fricke H, Reinicke O, Hofer H, Nachtigall W** (1987) Locomotion of the coelacanth *Latimeria*
747   *chalumnae* in its natural environment. *Nature* **329**, 331–333.

748 **Friedman M** (2007) *Styloichthys* as the oldest coelacanth: Implications for early osteichthyan
749   interrelationships. *J. Syst. Palaeontol.* **5**, 289–343.

750 **Friedman M, Brazeau MD** (2010) A reappraisal of the origin and basal radiation of the Osteichthyes.
751   *J. Vertebr. Paleontol.* **30**, 36–56.

752 **Friedman M, Coates MI** (2006) A newly recognized fossil coelacanth highlights the early
753   morphological diversification of the clade. *Proc. R. Soc. B Biol. Sci.* **273**, 245–250.

754   **Friedman M, Coates MI, Anderson P** (2007) First discovery of a primitive coelacanth fin fills a major
755   gap in the evolution of lobed fins and limbs. *Evol. Dev.* **9**, 329–337.

756   **Gosline WA** (1977) The structure and function of the dermal pectoral girdle in bony fishes with
757   particular reference to ostariophysines. *J. Zool.* **183**, 329–338.

758   **Grandel H, Schulte-Merker S** (1998) The development of the paired fins in the zebrafish (*Danio*
759   *rerio*). *Mech. Dev.* **79**, 99–120.

760   **Gregory WK, Raven HC** (1941) Part I: Paired Fins and Girdles in Ostracoderms, Placoderms, and
761   Other Primitive Fishes. *Ann. N. Y. Acad. Sci.* **42**, 275–291.

762   **Janvier P** (1996) *Early vertebrates*. Clarendon Press, Oxford.

763   **Jarvik E** (1980) *Basic structure and evolution of vertebrates*. Academic Press, New York.

764   **Johanson Z, Joss J, Boisvert CA, Ericsson R, Sujita M, Ahlberg PE** (2007) Fish fingers: Digit
765   Homologues in Sarcopterygian Fish Fins. *J. Exp. Zool. B. Mol. Dev. Evol.* **308**, 757–768.

766   **Johanson Z, Joss JM, Wood D** (2004) The scapulocoracoid of the Queensland lungfish *Neoceratodus*
767   *forsteri* (Dipnoi: Sarcopterygii): Morphology, development and evolutionary implications for
768   bony fishes (Osteichthyes). *Zoology* **107**, 93–109.

769   **Johanson Z, Long JA, Talent JA, Janvier P, Warren JW** (2006) Oldest coelacanth, from the Early
770   Devonian of Australia. *Biol. Lett.* **2**, 443–6.

771   **Jollie M** (1980) Development of Head and Pectoral Girdle Skeleton and Scales in *Acipenser*. *Copeia*
772   **1980**, 226–249.

773   **Joss J, Johanson Z** (2007) Is *Palaeospondylus gunni* a Fossil Larval Lungfish? Insights From
774   Neoceratodus forsteri Development. *J. Exp. Zool. B. Mol. Dev. Evol.* **308**, 163–171.

775   **Joss JM, Longhurst T** (2001) Lungfish paired fins. In: *Major events in early vertebrate evolution* (P. E.
776   Ahlberg, ed), pp. 289–306 London.

777   **Jude E, Johanson Z, Kearsley A, Friedman M** (2014) Early evolution of the lungfish pectoral-fin
778   endoskeleton: evidence from the Middle Devonian (Givetian) *Pentlandia macroptera*. *Front.*
779   *Earth Sci.* **2**, 1–15.

780   **Koumoundouros G, Divanach P, Kentouri M** (2001) Osteological development of *Dentex dentex*
781   (osteichthyes: Sparidae): Dorsal, anal, paired fins and squamation. *Mar. Biol.* **138**, 399–406.

782   **Lyckegaard A, Johnson G, Tafforeau P** (2011) Correction of Ring Artifacts in X-ray Tomographic

783   Images. *Int. J. Tomogr. Simul.* **18**, 1–9.

784   **Mabee PM** (2000) Developmental Data and Phylogenetic Systematics : Evolution of the Vertebrate
785   Limb. *Am. Zool.* **40**, 789–800.

786   **Mabee PM, Noordsy M** (2004) Development of the paired fins in the paddlefish, *Polyodon spathula*.
787   *J. Morphol.* **261**, 334–344.

788   **Manzano A, Abdala V, Ponssa ML, Soliz M** (2013) Ontogeny and tissue differentiation of the pelvic
789   girdle and hind limbs of anurans. *Acta Zool.* **94**, 420–436.

790   **McGonnell IM** (2001) The evolution of the pectoral girdle. *J. Anat.* **199**, 189–194.

791   **Millot J, Anthony J** (1958) *Anatomie de* Latimeria chalumnae*, Tome I : Squelette et Muscles*, CNRS.
792   Paris.

793   **Miyake T, Kumamoto M, Iwata M, *et al.*** (2016) The pectoral fin muscles of the coelacanth
794   *Latimeria chalumnae*: Functional and evolutionary implications for the fin-to-limb transition and
795   subsequent evolution of tetrapods. *Anat. Rec.* **299**, 1203–1223.

796   **Nagashima H, Kuraku S, Uchida K, Ohya YK, Narita Y, Kuratani S** (2007) On the carapacial ridge in
797   turtle embryos : its developmental origin , function and the chelonian body plan. *Development*
798   **134**, 2219–2226.

799   **Nakamura T, Gehrke AR, Lemberg J, Szymaszek J, Shubin NH** (2016) Digits and fin rays share
800   common developmental histories. *Nature* **537**, 225–228 Nature Publishing Group.

801   **Nowlan NC, Sharpe J** (2014) Joint shape morphogenesis precedes cavitation of the developing hip
802   joint. *J. Anat.* **224**, 482–489.

803   **Nulens R, Scott L, Herbin M** (2011) An updated inventory of all known specimens of the coelacanth,
804   *Latimeria* spp. *Smithiana Publ. Aquat. Biodivers.*, doi: 10.1109/TDEI.2009.5211872.

805   **Paganin D, Mayo SC, Gureyev TE, Miller PR, Wilkins SW** (2002) Simultaneous phase and amplitude
806   extraction from a single defocused image of a homogeneous object. *J. Microsc.* **206**, 33–40.

807   **Patterson C** (1982) Morphology and interrelationships of primitive actinopterygian fishes. *Integr.*
808   *Comp. Biol.* **22**, 241–259.

809   **Pierce SE, Clack JA, Hutchinson JR** (2012) Three-dimensional limb joint mobility in the early
810   tetrapod *Ichthyostega*. *Nature* **486**, 523–526.

811   **Pomikal C, Blumer R, Streicher J** (2011) Four-Dimensional Analysis of Early Pelvic Girdle

812   Development in *Rana temporaria*. **301**, 287–301.

813 **Pomikal C, Streicher J** (2010) 4D-Analysis of Early Pelvic Girdle Development in the Mouse (Mus
814   musculus). **126**, 116–126.

815 **Pouyaud L, Wirjoatmodjo S, Rachmatika I, Tjakrawidjaja A, Hadiaty R, Hadie W** (1999) A new
816   species of coelacanth. *Life Sci.* **322**, 261–267.

817 **Rocková H, Rocek Z** (2005) Development of the pelvis and posterior part of the vertebral column in
818   the Anura. *J. Anat.* **206**, 17–35.

819 **Rosen DE, Forey PL, Gardiner BG, Patterson C** (1981) Lungfishes, Tetrapods, Paleontology, and
820   Plesiomorphy. *Bull. Am. Museum Nat. Hist.* **167**, 159–276.

821 **Sanchez S, Ahlberg PE, Trinajstic KM, Mirone A, Tafforeau P** (2012) Three-dimensional synchrotron
822   virtual paleohistology: A new insight into the world of fossil bone microstructures. *Microsc.*
823   *Microanal.* **18**, 1095–1105.

824 **Schaeffer B** (1941) A revision of *Coelacanthus newarki* and notes on the evolution of the girdles and
825   basal plates of the median fins in the Coelacanthini. *Am. Museum Novit.* **1110**, 1–17.

826 **Schaeffer B** (1952) The Triassic coelacanth fish *Diplurus*, with observations on the evolution of the
827   Coelacanthini. *Bull. Am. Museum Nat. Hist.* **99**, 25–78.

828 **Shubin NH, Alberch P** (1986) A morphogenetic approach to the origin and basic organization of the
829   tetrapod limb. *Evol. Biol.* **20**, 319–387.

830 **Shubin NH, Daeschler EB, Jenkins FAJ** (2006) The pectoral fin of *Tiktaalik roseae* and the origin of
831   the tetrapod limb. *Nature* **440**.

832 **Smith JLB** (1939) A Living Fish of Mesozoic Type. *Nature* **143**, 455–456.

833 **Smith JLB** (1956) *Old Fourlegs: the Story of the Coelacanth*, Longmans G. London.

834 **Standen EM, Du TY, Larsson HCE** (2014) Developmental plasticity and the origin of tetrapods.
835   *Nature* **513**, 54–58 Nature Publishing Group.

836 **Stensiö EA** (1932) Triassic Fishes from East Greenland: Collected by the Danish Expeditions in 1929-
837   1931. *Meddelelser om Greenl.* **83**, 1–305.

838 **Stensiö EA** (1922) Über zwei Coelacanthiden aus dem Oberdevon von Wildungen. *Paläontologische*
839   *Zeitschrift* **4**, 167–210.

840 **Vickaryous MK, Hall BK** (2006) Homology of the reptilian coracoid and a reappraisal of the evolution

841   and development of the amniote pectoral apparatus. *J. Anat.* **208**, 263–285.

842   **Westoll TS** (1943) The origin of the tetrapods. *Biol. Rev.* **18**, 78–98.

843   **Zhu M, Schultze H-P** (2001) Interrelationships of basal osteichthyans. In: *Major events in early*
844   *vertebrate evolution* (P. E. Ahlberg, ed), pp. 289–306 London.

845   **Zhu M, Yu X** (2009) Stem sarcopterygians have primitive polybasal fin articulation. *Biol. Lett.* **5**,
846   372–375.

847   **Zhu M, Yu X, Choo B,** *et al.* (2012a) Fossil fishes from China provide first evidence of dermal pelvic
848   girdles in osteichthyans. *PLoS One* **7**.

849   **Zhu M, Yu X, Lu J, Qiao T, Zhao W, Jia L** (2012b) Earliest known coelacanth skull extends the range
850   of anatomically modern coelacanths to the Early Devonian. *Nat. Commun.* **3**, 772–778 Nature
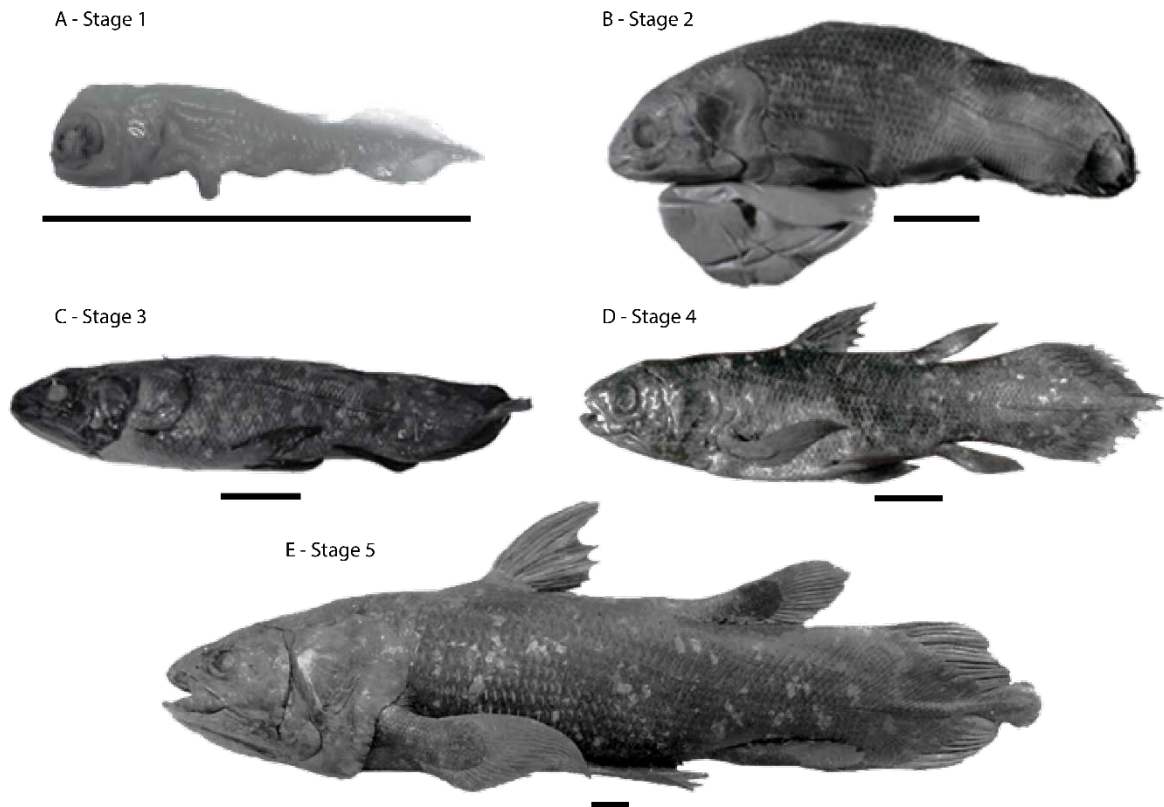851   Publishing Group.

852

Figure 1: Latimeria chalumnae - Ontogenetic series in left lateral view. A: Fetus (CCC 202.1), B: First pup (CCC 29.5), C: Second pup (CCC 162.21), D: Juvenile (CCC 94), E: Adult (CCC 22). Scale bar= 5 cm.
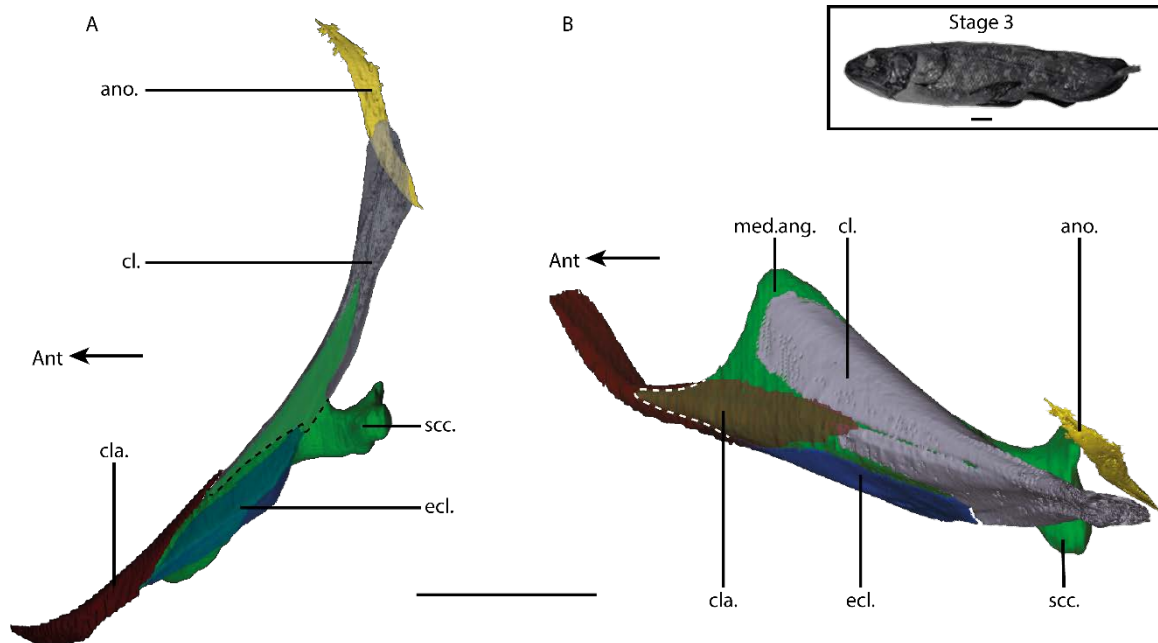

Figure 2: *Latimeria chalumnae* – Second pup. Left pectoral girdle in lateral (A) and dorsal (B) view. The cleithrum and extracleithrum are transparent in (A) to reveal the general shape of the scapulocoracoid; the clavicle is transparent in (B) to reveal the lateral angle of the scapulocoracoid. The dotted line shows the edge of the cleithrum in (A) and the edge of the scapulocoracoid in (B). ano. = anocleithrum; cl. = cleithrum; cla. = clavicle; ecl. = extracleithrum; lat.ang. = lateral angle of the scapulocoracoid; med.ang. = medial angle of the scapulocoracoid; scc. = scapulocoracoid. Scale bar = 20 mm.
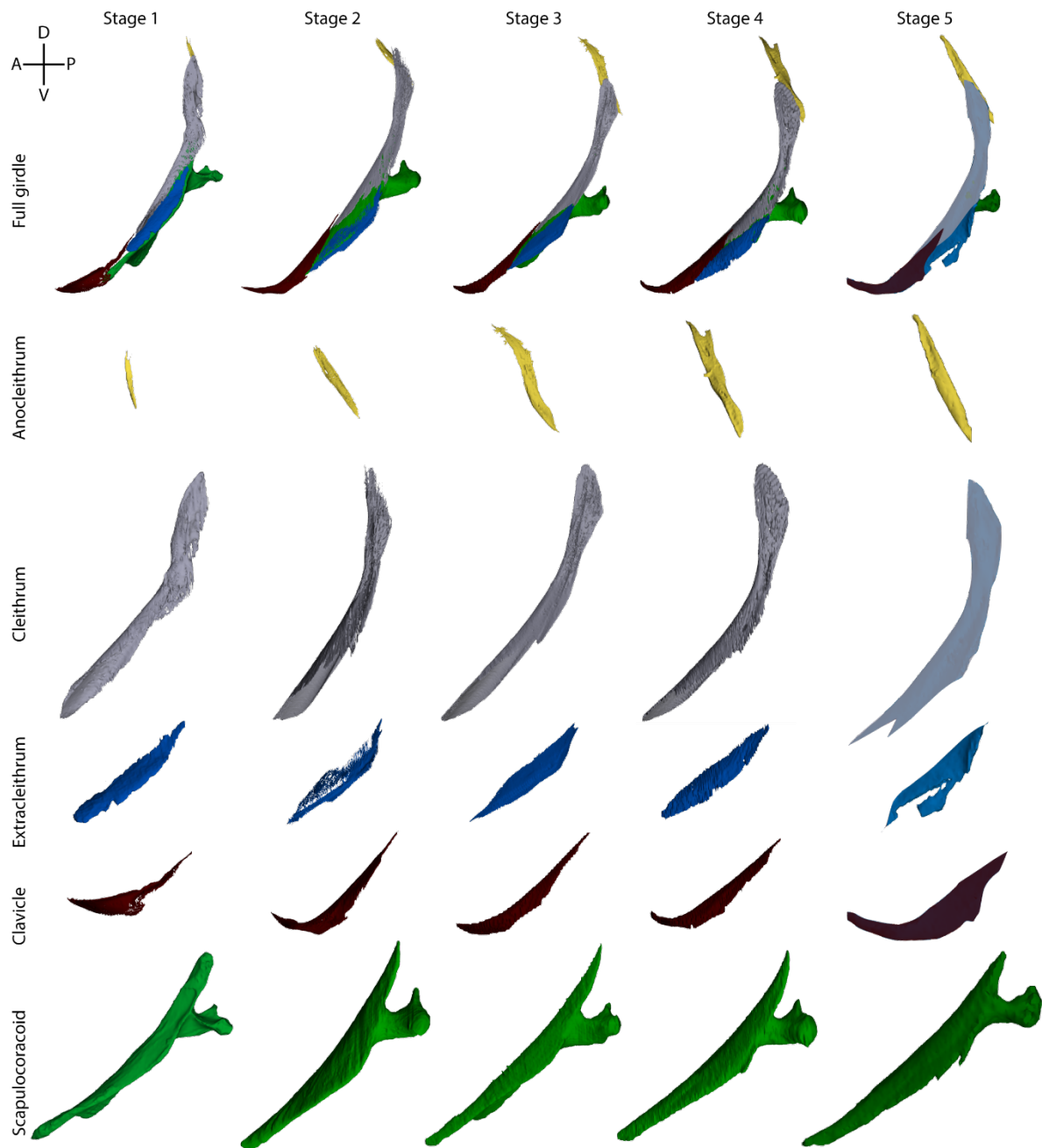
Figure 3: *Latimeria chalumnae.* Elements of the left pectoral girdle in lateral view at 5 different developmental stages (1 to 5). The different stages are not to scale, but the different bones within a given stage are to scale.
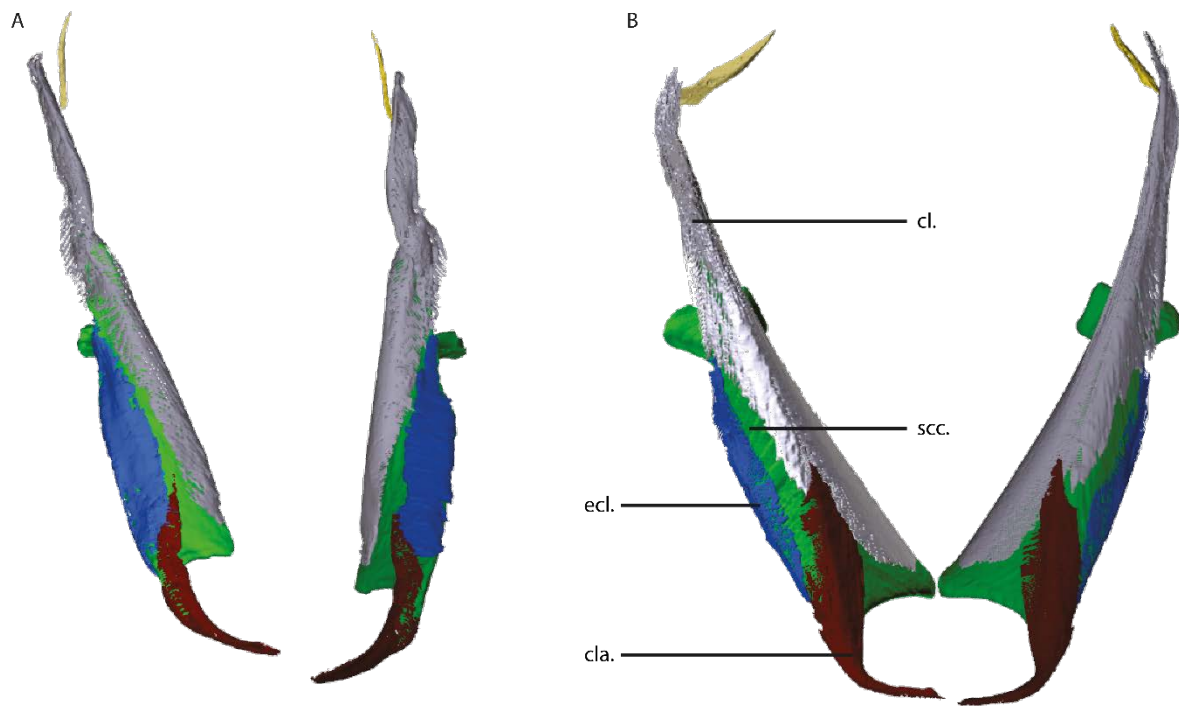
Figure 4: Latimeria chalumnae – The fetus and the first pup. Anterior views of the pectoral girdles of the fetus (A) and first pup (B) illustrating the reorientation of the pectoral girdles during the development of the coelacanth. cl. = cleithrum; cla. = clavicle; ecl. = extracleithrum; scc. = scapulocoracoid. Not to scale.
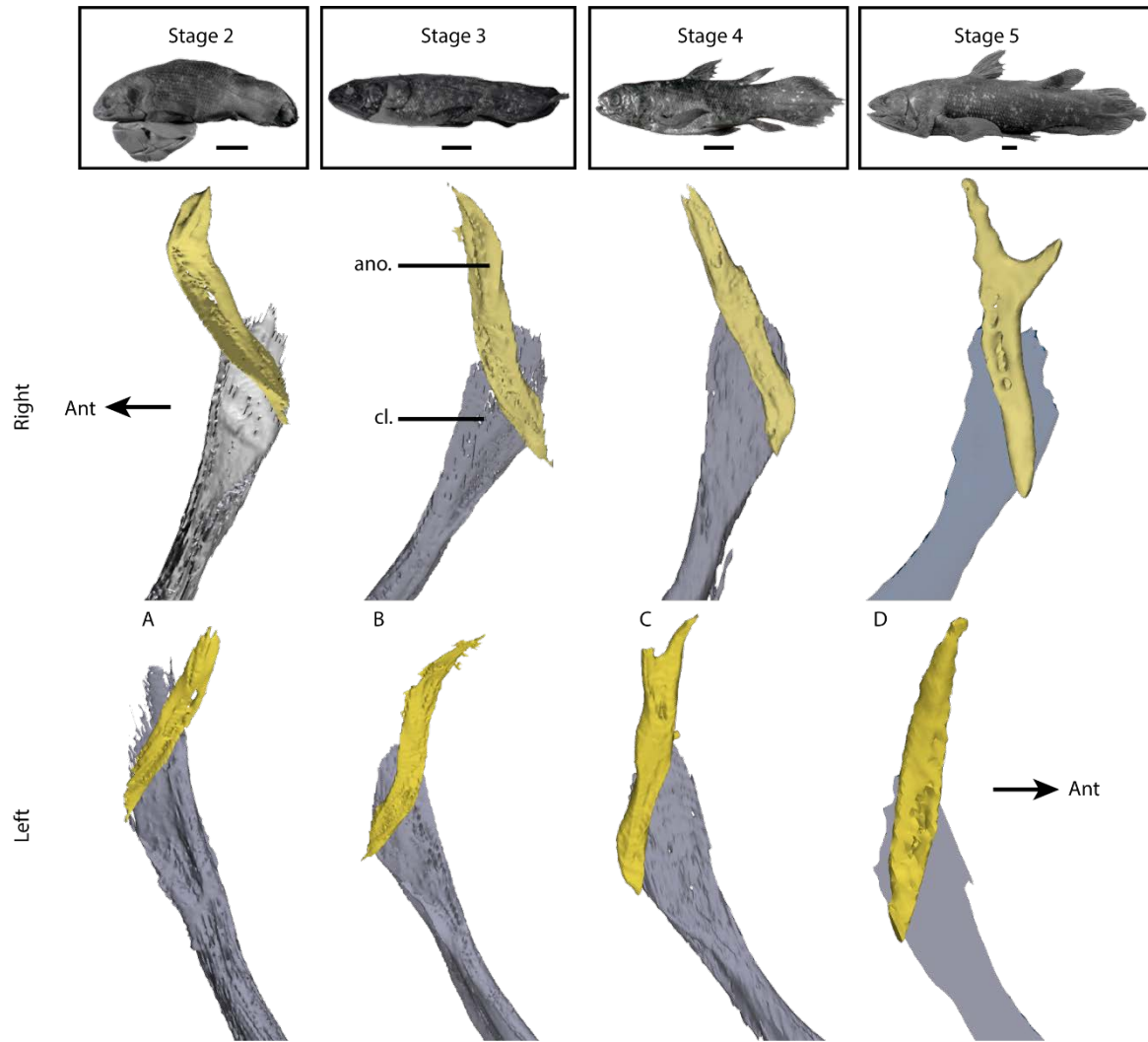
Figure 5: Latimeria chalumnae – Stage 2-5. Right anocleithrum (top) and left anocleithrum (bottom) in medial view. Note the intraspecific asymmetry and the individual asymmetry of the anocleithrum. ano. = anocleithrum; cl. = cleithrum. Scale bar = 5 cm. 3D models are not to scale.
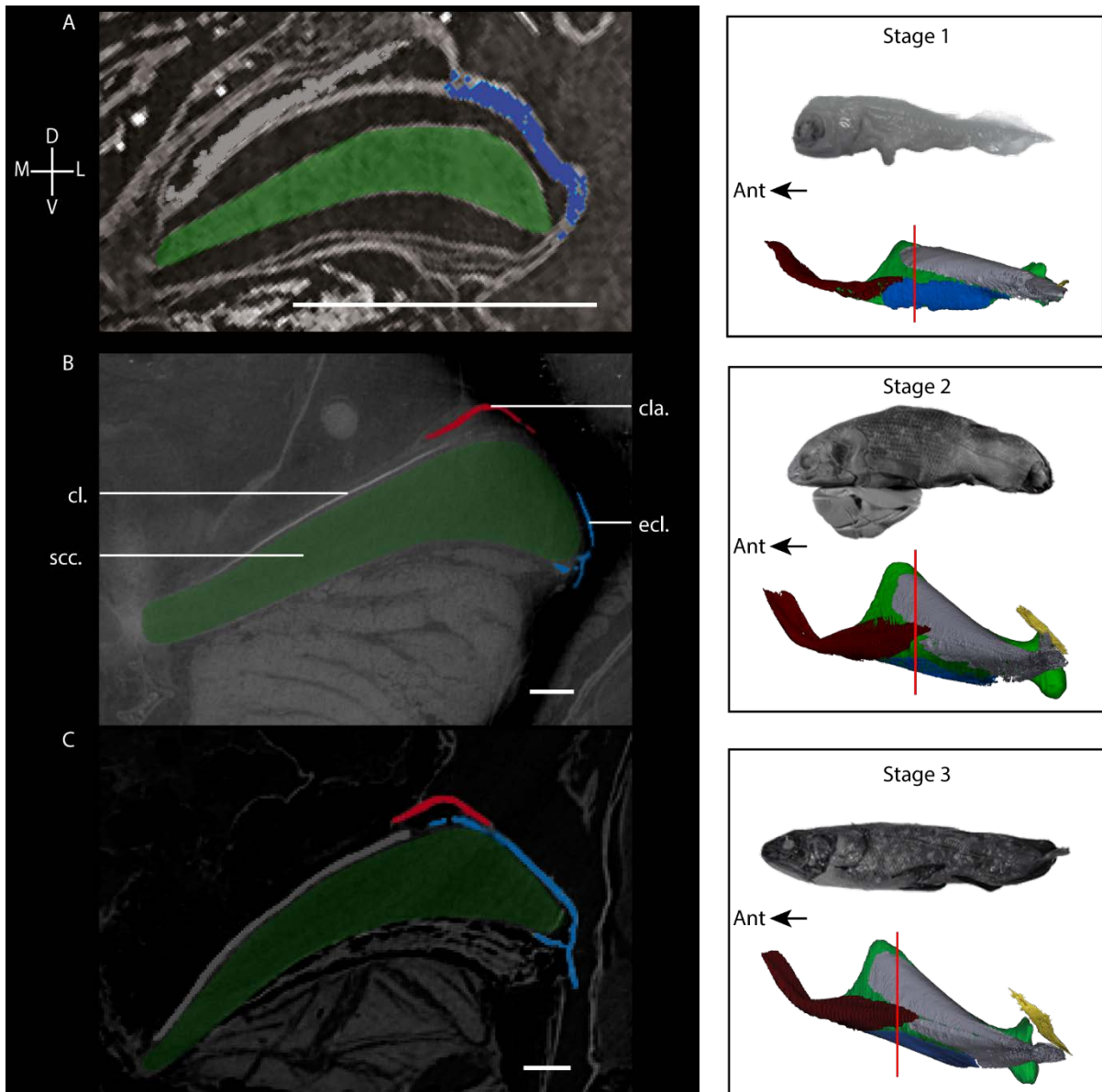
Figure 6: *Latimeria chalumnae* – The fetus (A), the first (B) and second (C) pup. Left pectoral girdle in transverse section. The location of the transverse sections are shown by a red line on the dorsal view of the 3D models of the pectoral girdles. In the fetus, the anterior part of the clavicle is not well developed and partially overlaps the posterior part of the cleithrum (not visible in the transverse section). In the first pup, the anterior part of the clavicle partially overlaps the cleithrum, but not the extracleithrum, whereas from the second pup onwards the anterior part of the clavicle partially covers both the cleithrum and the extracleithrum. cl. = cleithrum; cla. = clavicle; ecl. = extracleithrum; scc. = scapulocoracoid. D = dorsal; L = lateral; V= ventral; M = medial. Specimens and 3D models are not at scale. Scale bar = 1 mm.
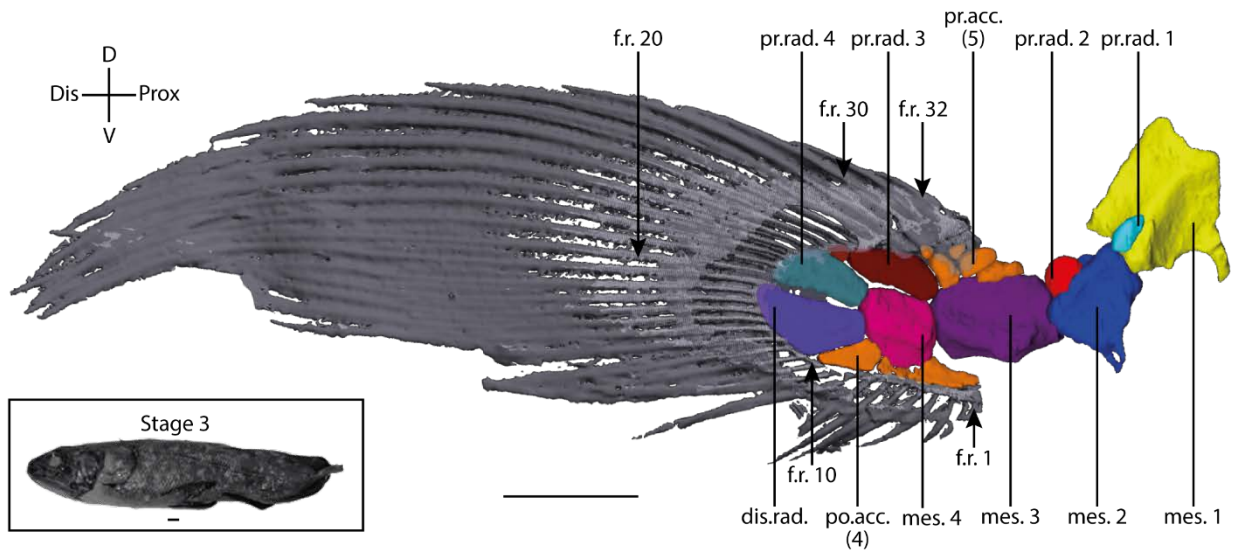
Figure 7: Latimeria chalumnae – Second pup. Right pectoral fin in lateral view. f.r. = fin ray; dis.rad. = distal radial; mes. = mesomere; po. acc. = post-axial accessory elements; pr. acc. = pre-axial accessory elements; pr. rad. = pre-axial radial. Scale bar = 10 mm.
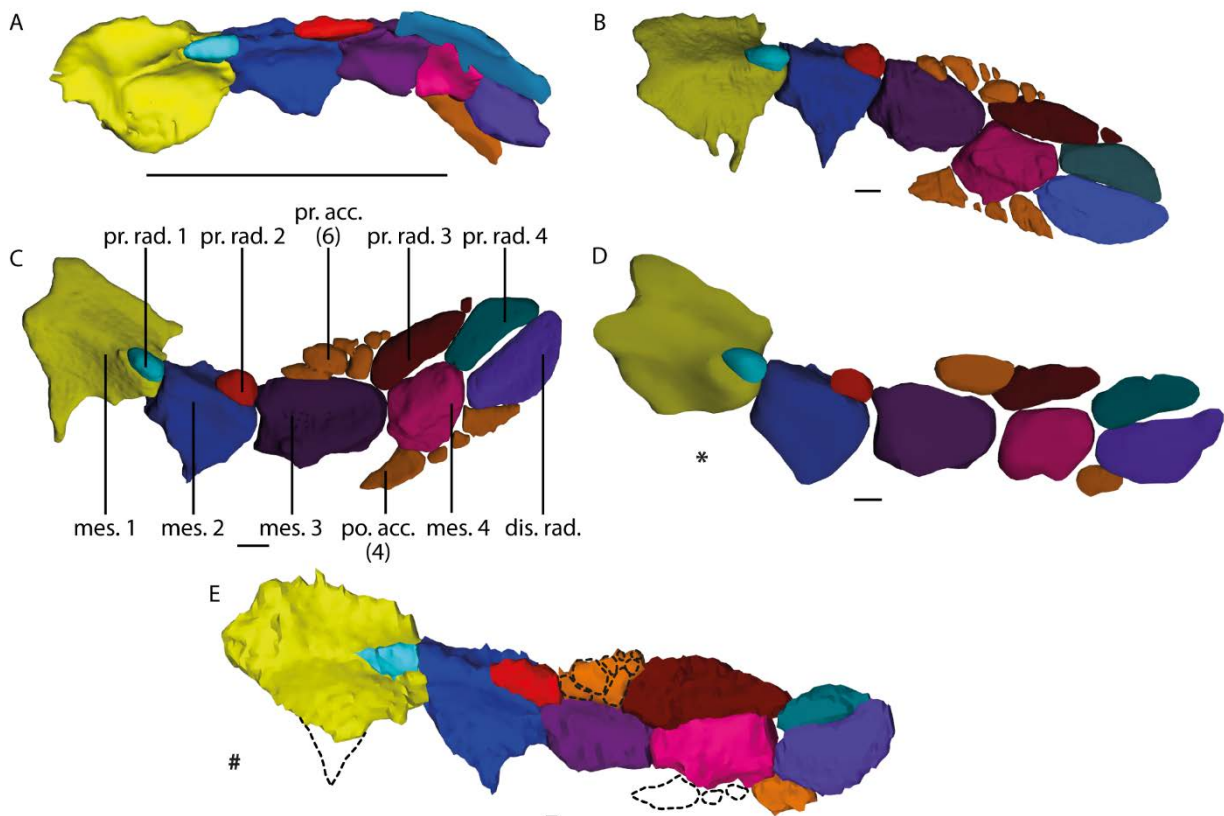

Figure 8: Latimeria chalumnae. Pectoral fin of five different developmental stages in left lateral view (B, C, D) and right lateral view (mirrored, A, E). A: the fetus, B: the first pup, C: the second pup, D: the juvenile, E: the adult. *: The juvenile was scanned with MRI at low resolution preventing the segmentation of the smallest elements. #: The adult was scanned using a regular CT-scan and the resolution of the data did not allow the segmentation of some elements. Corresponding elements of the fin have been indicated in the same color. The dotted line represents the pre-axial accessory elements, post-axial accessory elements and the hook on the mes. 1 of the stage 5 not segmented but known to exist based on prepared pectoral fins.

dis.rad. = distal radial; mes. = mesomere; po. acc. = post-axial accessory elements; pr. acc. = pre-axial accessory elements; pr. rad. = pre-axial radial. Scale bar = 2 mm (A), scale bar = 10 mm (B-E).
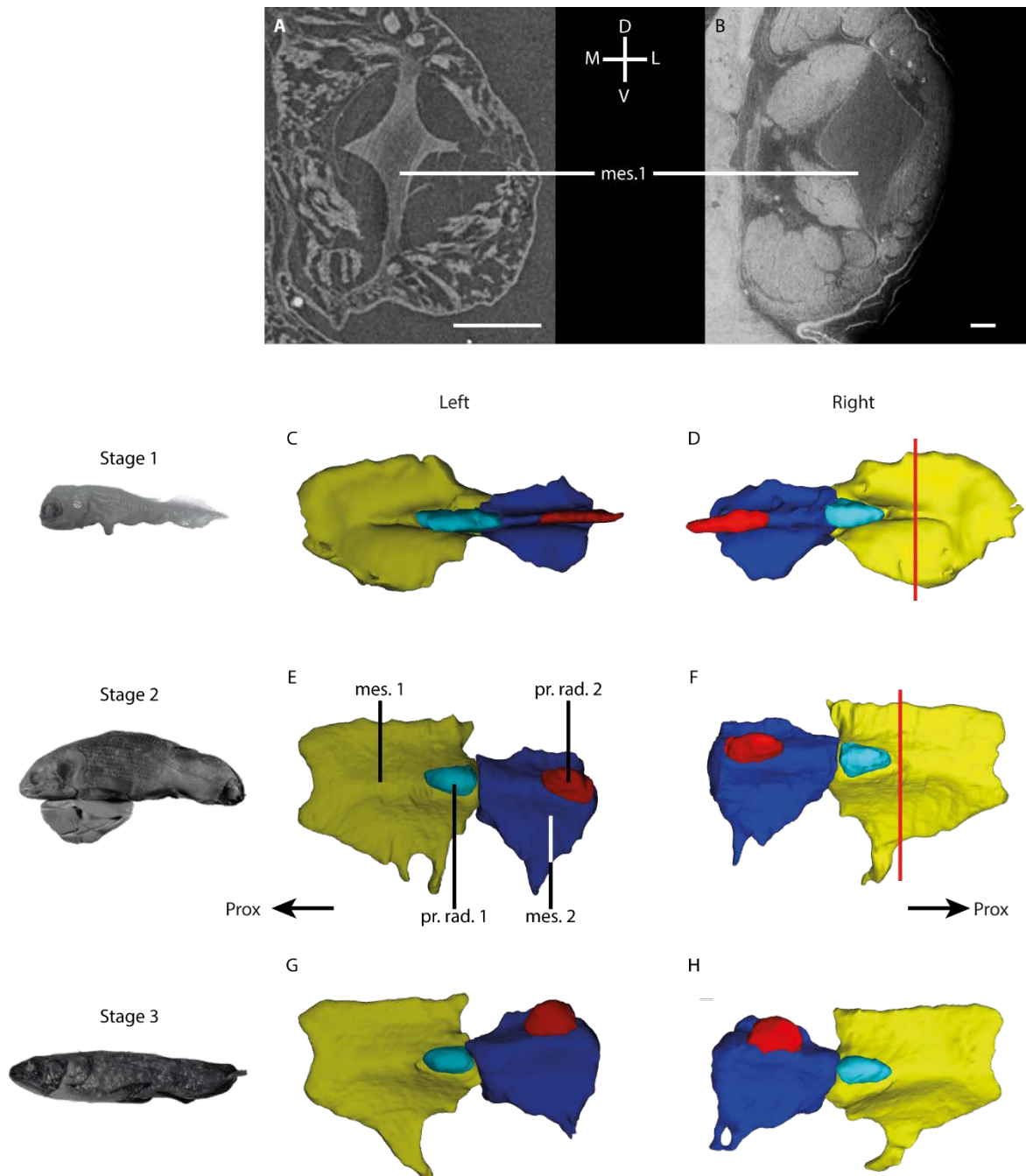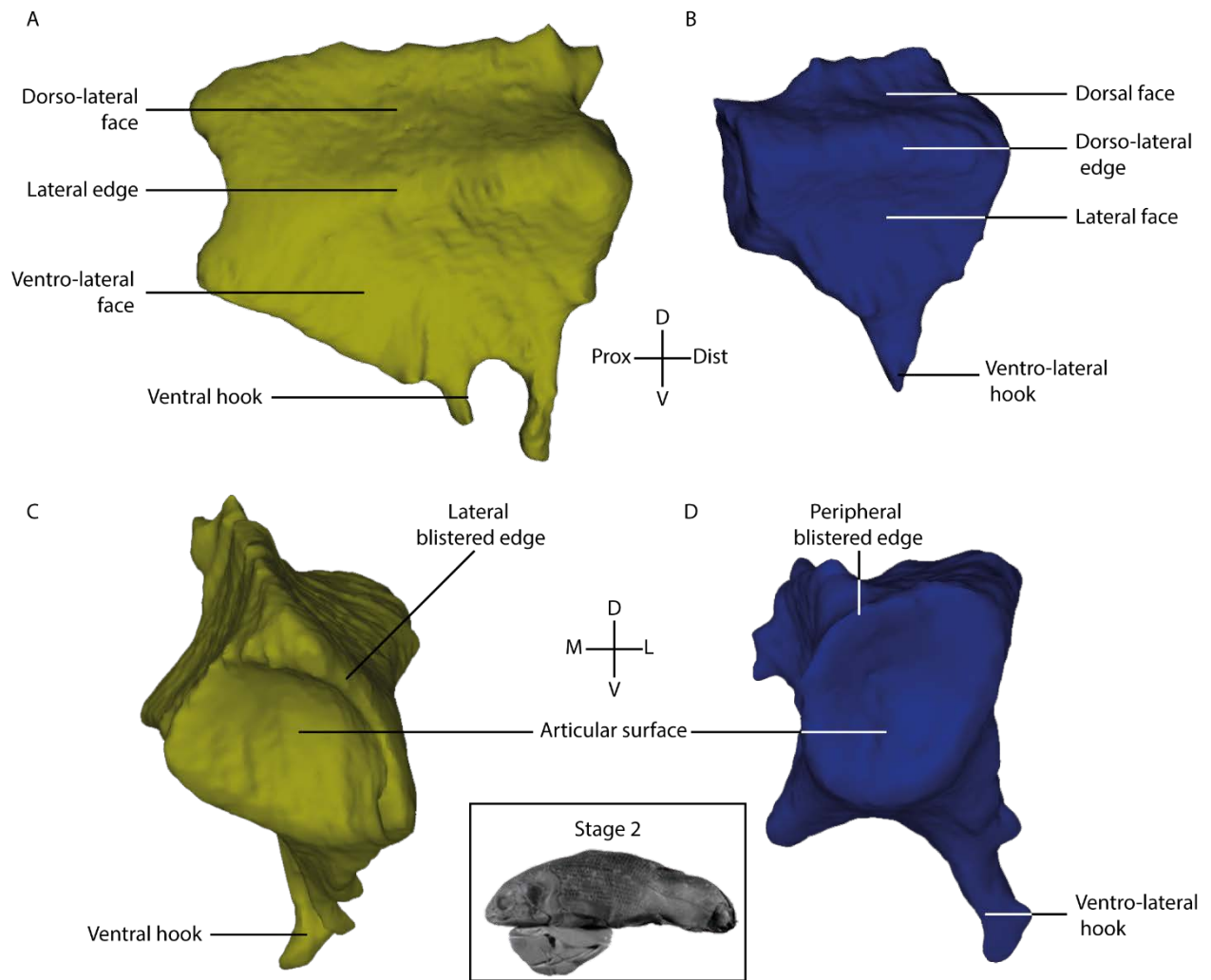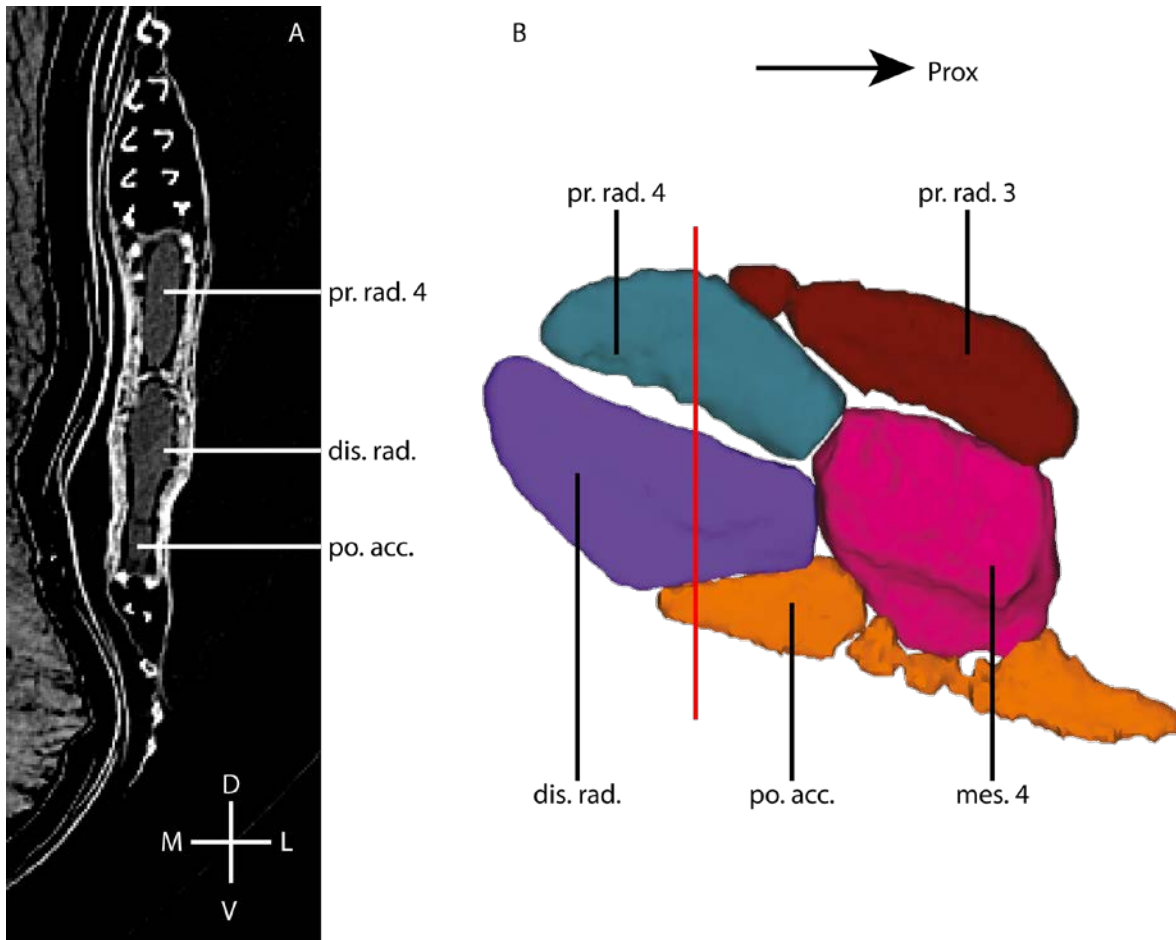

Figure 9: *Latimeria chalumnae* – Stages 1-3. Transverse sections of the first mesomere in the fetus (A) and the first pup (B), and lateral views of the left (C, E, G) and right (D, F, H) proximal elements of the pectoral fin of the fetus (C, D), the first pup (E, F) and the second pup (G, H). The location of the transverse sections are shown in the 3D models of the corresponding mesomeres (red line). In the fetus, the mesomeres have strongly concave faces (A, C, D), compared to the following stages (B, E-H). The pre-axial radial elements 1 and 2 are proportionally longer than in the next stages, and extend more distally than the end of the corresponding mesomere (C, D). In the first (E, F) and second pup (G, H), the pre-axial radial elements are proportionally shorter and have an ovoid shape. The left first mesomere of the first pup (E) shows a double hook on the ventral ridge, whereas the right first mesomere of first pup (F) and the first mesomeres of the second pup show only a single hook (G, H). The right second mesomere of the second pup (H) has a loop-like hook on the ventro-lateral edge whereas the

left second mesomere (G) and the second mesomere of the first pup (E, F) show a single hook. mes. = mesomere; pr. rad. = pre-axial radial. D = dorsal; L = lateral; M = medial; V= ventral. Scale bar = 1 mm. 3D models are not to scale.

Figure 10: *Latimeria chalumnae* – Stage 1-3. Distal part of the left (A, C, E) and right (B, D, F) pectoral fins of the fetus (A, B), the pup 1 (C, D) and the pup 2 (E, F) in lateral views. In the fetus, the right pectoral fin shows a large cartilaginous plate (blue) that corresponds to the pre-axial radials 3 and 4 and the pre-axial accessory elements in the following stages. The first and second pup show variation and asymmetry in the number of pre-axial accessory elements. dis.rad = distal radial; mes. = mesomere; po. acc. = post-axial accessory elements; pr. acc. = pre-axial accessory elements; pr. rad. = pre-axial radial. Not at scale.

SUPPLEMENTARY DATA

Supplementary Figure 1: Latimeria chalumnae – First pup. First (A, C) and second (B, D) mesomeres of the left pectoral fin in lateral view (A, B) and proximal view (C, D). The lateral view of the two mesomeres shows the different faces and the reorientation of the mesomeres along the axis. The proximal view shows the different articular surfaces of the first and second mesomeres. D = dorsal; L = lateral; M = medial; V= ventral. Not to scale.

Supplementary Figure 2: *Latimeria chalumnae* – Second pup. Transverse section of the distal end of the right fin (A) and its location on the lateral view of the 3D model (B). The distal radial presents only two convex faces, different from the previous axial elements of the fin that have four concave faces. dis.rad = distal radial; mes. = mesomere; po. acc. = post-axial accessory elements; pr. rad. = pre-axial radial. D = dorsal; L = lateral; M = medial; V= ventral. Not to scale.